Optimized detection of allelic imbalances specific for homologous recombination deficiency improves the prediction of clinical outcomes in cancer

Fernando Perez-Villatoro[1,2], Jaana Oikkonen[1], Julia Casado[1,2], Anastasiya Chernenko[1,2], Doga C. Gulhan[3], Manuela Tumiati[1], Yilin Li[1], Kari Lavikka[1], Sakari Hietanen[4], Johanna Hynninen[4], Ulla-Maija Haltia[5], Jaakko S. Tyrmi[6,7], Hannele Laivuori[6], Panagiotis Konstantinopoulos[9], Sampsa Hautaniemi[1], Liisa Kauppi[1,8], Anniina Färkkilä[1,2,5,9]

[1] Research Program for Systems Oncology, University of Helsinki, Helsinki, Finland
[2] iCAN digital precision cancer medicine flagship
[3] Department of Biomedical Informatics and Ludwig Center at Harvard, Harvard Medical School, Boston, MA, USA
[4] Department of Obstetrics and Gynecology, University of Turku and Turku University Hospital, Turku, Finland
[5] Department of Obstetrics and Gynecology, Helsinki University Hospital, Helsinki, Finland
[6] Faculty of Medicine and Health Technology, Center for Child, Adolescent, and Maternal Health, Tampere University Tampere, Finland
[7] Computational Medicine, Faculty of Medicine, University of Oulu, Oulu, Finland
[8] Department of Biochemistry and Developmental Biology, University of Helsinki, Helsinki, Finland
[9] Dana-Farber Cancer Institute, Harvard Medical School, Boston, USA

Correspondence:
Anniina Färkkilä, MD PhD, Docent in Translational Gynecologic Oncology
Principal Investigator, Academy of Finland Clinical Research Fellow
Specialist in Obstetrics and Gynecology

Research Program for Systems Oncology &
Department of Obstetrics and Gynecology
University of Helsinki and Helsinki University Hospital
00014 University of Helsinki
anniina.farkkila@helsinki.fi
+358505967786

ABSTRACT

Homologous recombination DNA-repair deficiency (HRD) is a common driver of genomic instability and confers a therapeutic vulnerability in human cancer. Using a systematic pan-cancer characterization, we revealed distinct patterns of somatic allelic imbalances (AIs) in high-grade serous ovarian cancer (HGSC). Using machine learning on a multi-omics dataset, we generated an optimized algorithm to detect HRD in HGSC (ovaHRDscar). ovaHRDscar improved the prediction of clinical outcomes in three independent validation cohorts. Characterization of 98 spatiotemporally distinct tumor samples indicated ovary/adnex as the preferred site to assess HRD. Cancer-specific optimization improved the prediction of clinical outcomes also in triple-negative breast cancer (tnbcHRDscar). In conclusion, our systematic approach based on multi-omics data improves the detection of HRD with the premise to improve patient selection for HR-targeted therapies.

INTRODUCTION

As a part of the Fanconi Anemia (FA) pathway, homologous recombination (HR) is an evolutionarily conserved, tightly regulated mechanism for high-fidelity repair of DNA double strand breaks (DSBs)[1]. Deficiency in homologous recombination (HRD) has profound consequences for replicating cells driving genomic instability and oncogenic transformation. In cancer, HRD results in a fundamental vulnerability, and tumors with HRD are markedly sensitive to DSB-inducing agents such as platinum-based chemotherapy and Poly-ADP Ribose Polymerase (PARP) inhibitors[2].

High-grade serous ovarian, peritoneal or fallopian tube cancer (HGSC), the most common and most lethal subtype of ovarian cancers[3], is characterized by profound genomic instability. Around half of the HGSCs are considered to harbor genomic alterations leading to HRD[4], and these patients have been shown to significantly benefit from treatment with PARP inhibitors[5,6]. The HRD test used in PARP inhibitor clinical trials[5,6] is based on the quantification of specific allelic imbalances (AIs): 1) Large scale transitions (LSTs)[7], 2) Loss of heterozygosity (LOH)[8] and 3) Telomeric allelic imbalances (TAIs)[9]. However, the defining criteria for these HRD specific AIs (HRD-AIs) were originally designed using mostly breast cancer, or in a mixture of breast and ovarian cancer samples[7,8,9]. Therefore, the details of the genomic instability occurring due to HRD in HGSCs have not been clearly defined. Herein, we show that HGSC harbors distinct patterns of AIs as compared to other cancer types, including triple negative breast cancer (TNBC). Using a systematic approach based on machine learning and statistics on The Cancer Genome Atlas (OVA-TCGA) multi-omics dataset, we optimize the defining criteria of HRD-AIs for HGSC and present an algorithm (ovaHRDscar) to reliably define HRD status. We show that ovaHRDscar improves the detection of HRD and prediction of therapy responses and clinical outcomes in three independent clinical datasets as compared to previous algorithms. Further, we show that our systematic and disease-specific approach

improves the prediction of clinical outcomes in TNBC. HRDscar thus shows promise as an optimized biomarker that can be used to improve outcome prediction and patient selection for HR-targeted therapies in cancer.

RESULTS

Systematic PanCancer characterization reveals unique features of allelic imbalances in HGSC

To elucidate the potential differences in AI patterns in human cancers, we first characterized the quantity and size distributions of AIs in eighteen most common cancer types from the TCGA (**Fig. 1a**). Interestingly, HGSC had the highest number of AIs (**Fig. 1b**), but the AIs were of the lowest median size as compared to the other tumor types (**Fig. 1c**). Concordantly, HGSCs showed the highest levels of LOH events (**Supplementary Fig. 1a**) with one of the lowest median LOH sizes (**Supplementary Fig. 1b).**

We next performed hierarchical clustering using the median value of AI length per sample, median value of AI number per sample and the skewness of the size distribution for each cancer type. Cancer types were clustered in two main clusters, one of those consisting of six cancer types (BLCA, STAD, LUSC, BRCA, LUAD, and HGSC) with a higher amount but a lower median length of the AIs (upper cluster: **Fig. 1d**) and the second cluster conformed by the remaining twelve types of cancers (lower cluster: **Fig. 1d**). The same main clusters were generated when using only LOH events (**Supplementary Fig. 1c**).

As TNBC and HGSC are enriched in *BRCA* gene mutations[11], and both cancers were used to define the HRD test used in clinical assays[10], we next compared the differences in AIs between these two cancer types. We observed a significant difference in the abundance of AIs between HGSC cancer and TNBC, specifically in *BRCA*-wild-type *(BRCA*wt*)* tumors (U test, $p = 0.005$, **Fig. 1g**), but not *BRCA*-mutated *(BRCA*mut*)* tumors (**Fig. 1f**). Interestingly, HGSCs had lower

levels of LOH events than TNBCs (U test, p = 0.008, **Supplementary Fig. 1d**), also among the *BRCA*mut samples (U test, p = 0.021, **Supplementary Fig. 1e**) but not in *BRCA*wt samples (**Supplementary Fig. 1f**). We then compared the numbers of AIs of different sizes between HGSC and TNBC. Overall, HGSCs showed higher levels of AIs of different sizes while TNBC had higher levels of LOH events (**Fig. 1h**). Interestingly, LOH events of a size from 16 to 22Mb and longer than 30Mb were in higher proportion in TNBC in *BRCA*mut samples, while AIs shorter than 30Mb were in higher proportions in HGSC. These results highlight the different characteristics of AI events in HGSCs, especially *BRCA*wt tumors, as compared to other cancer types.

Optimized ovaHRDscar improves the detection of HRD in HGSC

Although a wide range of molecular alterations are known to cause HRD, previous studies have focused on *BRCA* mutations to detect HRD specific AIs (HRD-AIs) potentially failing to detect non-BRCA associated HRD alterations, while losing specificity to accurately classify the HRP samples. To this end, we aimed to identify AIs overrepresented in samples carrying a wider range of genetic alterations (mutations, gene deletions, promoter hypermethylation) associated with HRD in HGSC (**Fig. 2a**). To optimize the size selection criteria of HRD-AIs, we utilized SNP Array data from HGSC samples from TCGA (OVA-TCGA) and its associated genomic and DNA methylation data. Via an approach (Methods) utilizing prior knowledge and multi-omics data, we identified (annotated) 115 HRD samples harboring a somatic or germline mutation, gene deletion or promoter hypermethylation in the *BRCA1/2* or *RAD51* paralog genes, and 29 HR-proficient (HRP) samples that did not harbor any of the alterations used to select HRD samples, nor deletion in any other HR gene (**Fig. 2a**). A detailed description of the genomic alterations in the samples is reported in **Supplementary Table 1**. Overall, HRD samples had a higher amount of all AIs than HRP samples (U test, p = 0.0028, **Supplementary Fig. 2a**). Importantly, HRD samples had a notably higher proportion of AIs with specific sizes that span from 1Mb to 30Mbs (**Supplementary Figs. 2b, c**), while the HRP samples contained a higher proportion of AIs and LOH events smaller than 1Mb.

We next applied an systematic approach (Methods) to identify the specific of LOH, LST and TAI events overrepresented in HRD samples by using statistics and machine learning (**Fig. 2b**). This systematic approach selects AIs of with given criteria (Methods), then calculates independently 1) the difference in abundance of the selected AIs between the annotated HRD versus HRP samples and 2) the classification accuracy of the annotated HRD from HRP samples by machine learning decision trees[12], taking abundance of AIs as the splitting criterion. AIs selecting criteria that produced the highest difference in both abundance and accuracy were selected. The approach allowed us to optimize the HRD-AIs size selection for LOH, LST and TAI which are distinct in HGSC as compared to the HRD score used previously in clinical trials (hereafter called Telli2016). Notably, for LSTs our approach increased the accuracy of classification of the HRD/HRP samples from 86% to 90% when using the optimized cut-offs (**Fig. 2c**). For LOH events, the accuracy increased from 85% to 88% when using the optimized criteria (**Supplementary Fig. 2d**). We also assessed the classification accuracy of LSTs consisting of three consecutive AIs, however this produced a lower accuracy (**Supplementary Fig. 2e**). Similarly, for TAI events, the accuracy increased from 67% to 78% (**Supplementary Fig. 2f**). As the largest improvement in accuracy of TAI occurred after including TAIs larger than 1Mb, and inclusion of bigger sizes did not increase considerably the accuracy, we decided to ignore TAIs smaller than 1Mb rather than selecting TAIs with a specific size.

Via our systematic approach, we observed the following AIs to be most characteristic of HRD in HGSC: 1) LOH > 15Mb and <50Mb, 2) for LSTs AI > 12Mb with a space between them <1Mb and 3) TAI >1Mb. The sum of these events is hereafter called the ovaHRDscar levels. Then, using bootstrapping subsampling of the pre-selected HRD and HRP samples we evaluated the optimal ovaHRDscar cutoff value to define HR-status. The value with the highest balanced accuracy (BA) was 54 (**Fig. 2d**), meaning that values higher or equal than 54

correspond to HRD, with a higher accuracy for HR-status classification (BA=0.89, right panel **Fig. 2e**) as compared to the Telli2016 algorithm (BA=0.76, left panel **Fig. 2e**).

ovaHRDscar levels correlate with genomic features of HRD and show concordance in WGS data

In order to investigate the relationships of ovaHRDscar with other known genomic features associated with HRD, we annotated the OVA-TCGA samples according to mutations, gene deletions and promoter hypermethylation patterns previously reported associated with HRD[4] (**Fig. 2f**). On average, samples with somatic mutations in *BRCA1*, *BRCA2*, *PTEN*, or somatic mutations or gene deletions in any gene belonging to the Fanconi Anemia (FA) or HR pathways showed high ovaHRDscar levels. Likewise, samples that contained hypermethylation in the promoter regions of *BRCA1* or *RAD51C* genes, or germline mutations in *BRCA1* or *BRCA2* had on average high ovaHRDscar levels. As expected, samples harboring an amplification in *CCNE1* (**Supplementary Fig. 2g**) had significantly lower levels of ovaHRDscar. In addition to *BRCA1/2* or *RAD51* paralogs, samples with molecular alterations previously associated with HRD contained on average significantly higher levels of ovaHRDscar as compared to the samples with *CCNE1* amplification (**Supplementary Fig. 2g**). However, samples with *EMSY* amplification and *CDK12* somatic mutation presented with low ovaHRDscar levels (**Supplementary Fig. 2g**).

To assess the concordance of ovaHRDscar in whole genome sequencing (WGS) data and mutational signatures, we next quantified the ovaHRDscar levels in HGSC samples from the Pan-Cancer Analysis of Whole Genomes project (PCAWG)[13]. First, we evaluated the level of agreement of the ovaHRDscar levels between WGS and SNP-array data. For this we selected 41 OVA-TCGA samples that were also included in the PCAWG project. The ovaHRDscar levels were highly concordant between WGS and SNP-arrays (Lin's concordance correlation coefficient, ccc = 0.90; **Supplementary Fig. 2h**), this is consistent with a previous report in breast cancer samples that quantified AIs in the two platforms[14]. Next, we tested the

correlation of ovaHRDscar with the single base substitution signature 3 (SBS3), which has been associated with HRD in human cancers samples[15]. We found that ovaHRDscar levels detected in WGS positively correlated with the proportion of SBS3 in WGS (Pearson, r'=0.38, p= 3.7e-05; **Fig. 2g**). The SBS3 proportions also correlated with the number of HRD-AIs using the Telli2016 algorithm in PCAWG (**Supplementary Fig. 2i**).

SBS3 has also been inferred from whole exome sequencing (WES) data with a likelihood-based approach SigMA[16]. We next compared the performance of ovaHRDscar to that of SBS3 status inferred from WES in OVA-TCGA. The ovaHRDscar algorithm detected a total 145 samples as HRD (57%) and the SigMA tool classified 142 samples (56%) as SBS3+; in comparison, the Telli2016 algorithm identified 220 samples (83%) as HRD (**Fig. 2h**). HRD detection with ovaHRDscar showed an improved agreement with SigMA (agreement 78.3% and cohen's kappa = 0.56) as compared to the Telli2016 algorithm (agreement 68.5% and cohen's kappa = 0.32; **Fig. 2h**).

ovaHRDscar improves the prediction of PFS and OS compared to previous algorithms

Next, we measured the association of HR-status classification by ovaHRDscar to progression-free survival (PFS, see methods) in HGSC patients treated with platinum-based chemotherapy in TCGA and in an independent validation dataset (HERCULES). We compared the performance of ovaHRDscar versus *BRCA1/2* deficiency status, the Telli2016 algorithm, and to an HRD/HRP cutoff value of 63 HRD-Ais, as proposed by Tacaya et al[17]. As *BRCA1/2* mutations can affect patient outcomes, we assessed the performances of ovaHRDscar in the TCGA also after excluding the samples used in the training set, even though clinical outcomes were not utilized for the optimization. *BRCA1/2* mutation or deletion status (*BRCA*mut/del) was not significantly associated with PFS (log-rank p=0.72; **Fig. 3a**). For OVA-TCGA (**Fig. 3a to 3c**), we found that ovaHRDscar positivity was associated with prolonged PFS (log-rank p=4.4e−04; **Fig. 3c**) with smaller 95% confidence intervals and a lower p-value as compared

to the Telli2016 algorithm (log-rank p=0.017; **Fig. 3b**); the median PFS was 19.8 months for the ovaHRDscar positive patients and 17.9 months for the Telli2016 positive patients. Consistently, also in the HERCULES cohort, ovaHRDscar positive patients had a longer PFS (log-rank p=0.001; **Supplementary Fig. 3c**), while the Telli2016 algorithm did not reach statistical significance in predicting PFS (log-rank p=0.07; **Supplementary Fig. 3b**).

Residual tumor after primary debulking surgery has been shown to be a strong independent prognostic factor[18], and we next used Cox proportional hazard models to assess the performance of HRD algorithms in predicting PFS. We found that ovaHRDcar positivity was associated most significantly with prolonged PFS in OVA-TCGA when adjusting for residual tumor (Wald test p=1.5e−07, **Fig. 3d**) outperforming the Telli2016 algorithm (Wald test p=2.7e−06) and the Tacaya algorithm (Wald test p=1.2e−06). The same was true also after excluding the samples used in the optimization (middle panel, **Fig. 3d**) and when not adjusting for the residual tumor (**Supplementary Fig. 3d**). In contrast to previous algorithms, ovaHRDscar positivity was associated with longer PFS in the Cox models also in the independent HERCULES cohort (HR 0.37, Wald test p=0.013). Results were similar after excluding the *BRCA*mut/del samples from the cohorts (Lower panel, **Fig. 3d**). We inspected the performance of HRD-classification algorithms in a second independent prospective cohort (TERVA) with tumor-only SNP array profiling, performed with a panel of normals (see methods). Importantly, ovaHRDscar positivity most significantly predicted longer PFS using log-rank test and cox proportional hazard model (**Supplementary Fig. 3e to 3g**). For most of the comparisons these results were consistent in the non-adjusted Cox regression models (**Supplementary Fig. 3e**).

Subsequently, we explored the association of ovaHRDscar with overall survival (OS) in HGSC patients in the OVA-TCGA cohort, and in an independent AU-OVA cohort in PCAWG. The clinical data in the prospective cohorts (HERCULES, TERVA) were not mature enough for OS evaluation. We found that both in the OVA-TCGA and PCAWG datasets, ovaHRDscar was

superior to *BRCA1/2* deficiency status, and to Telli2016 or Tacaya2020 algorithms (**Fig. 3g, Supplementary Fig. 3j**). In Cox regression analysis for OS using patient age at diagnosis as a covariable, ovaHRDscar had improved significance for predicting OS (**Fig. 3h**). Of note, the hazard-ratio values were lower in OVA-TCGA using the Telli2016 algorithm; however, the corresponding hazard ratio was not significant in the PCAWG cohort. Consistent with PFS analysis, the ovaHRDscar hazard-ratios and significance were superior to the Tacaya2020 algorithm in all comparisons. These results were concordant also using a non-adjusted Cox regression analysis (**Supplementary Fig. 3k**). Additionally, we compared the performance of ovaHRDscar to the CHROD algorithm that uses structural variations and a random forest implementation to classify HR-status[19]. We found that ovaHRDscar showed an improved prediction of OS as compared to the CHORD algorithm using log-rank test (**Supplementary Fig. 3l, m**) and using Cox proportional hazard models (**Supplementary Fig. 3n**) in the PCAWG cohort.

Low intra-patient variation of ovaHRDscar in spatiotemporal tumor profiling

HGSC is characterized by high intertumor heterogeneity, and we next explored whether the anatomical site or timing of sample retrieval affects HR-status classification in HGSC. For this, we explored the concordance of ovaHRDscar levels in the HERCULES prospective cohort, which included 89 tumor samples from different anatomical sites and different treatment phases (treatment-naive, after neoadjuvant chemotherapy, or at relapse) from 33 HGSC patients (**Fig. 4a**). Consistent with the TCGA dataset, ovaHRDscar levels corresponded with known genomic predictors of HR-status (**Fig. 4b**). Importantly, we found that the levels were similar in paired, anatomically matched samples obtained before and after neoadjuvant chemotherapy, and also in primary (treatment-naive) versus relapsed tumors (**Fig. 4c**). Further, the intra-patient levels variability was not explained by differences in tumor purity (minimum 30%, see methods) (**Supplementary Fig. 4b** and **Supplementary Fig. 4c**). We observed some intra-patient variation between anatomical sites (**Fig. 4a**), however it was lower than the inter-patient variation (U test p=1.95e-38**; Supplementary Fig. 4a**). To

determine the optimal anatomical sampling site, we next assessed HR-status per patient in treatment-naive primary samples and compared ovaHRDscar calculated from specific anatomical sites (or average if many samples per site) including 1) all samples (All) 2) ovarian (OVA) 3) ovarian or adnexal (OVA/ADN) 4) omentum, and OVA/ADN if omentum sample not available (OME-OVA/ADN) 5) OVA/ADN, and then omentum if OVA/ADN not available (OVA/ADN-OME). Overall, the level of agreement for the HR-status classification between the prioritization of anatomical sites ranged from 94% and 97% (**Supplementary Fig. 4d**). Notably, ovaHRDscar status calculated primarily from ovarian or adnexal tumor was the strongest predictor for PFS (**Fig. 4d**, **Supplementary Fig. 4e**). Consistently, prioritizing ovarian tumors (OVA) accurately classified all tumors harboring *CCNE1* amplification as HRP in the prospective HERCULES cohort (**Supplementary Fig. 4d**).

HRD-AI optimization improves the prediction of clinical outcomes in TNBC

Finally, we tested if our systematic optimization of HRD-AIs could improve previous algorithms when predicting clinical outcomes also in TNBC. For this, using multi-omics data in TCGA and the same classification approach (**Fig. 2a**), we identified 47 TNBCs as HRD and 23 as HRP (**Fig. 5a**). Optimization of LOH increased the accuracy of classification of HR-status from 80% (Telli2016 algorithm) to 93% (**Fig. 5b**). Likewise, for LSTs the optimization increased accuracy from 93% to 98% (**Supplementary Fig. 5a**) and for TAIs from 86% to 92% (**Supplementary Fig. 5b**). Similarly as for HGSC, instead of selecting TAIs of a particular size we selected TAIs bigger than 1Mb as this resulted in the largest increase in significance. The following HRD-AI criteria were observed most characteristic in TNBC: 1) LOH >10Mb and <30Mb, 2) for LSTs AI >5Mb with a space between them <2Mb, and 3) TAI >1Mb. Then, using a subsampling approach we identified that cut-off values for the sum of HRD-AIs (hereafter called tnbcHRDscar) from 47 to 53 produced the highest classification accuracy of the HRD and HRP samples (**Fig. 5c**), with the cut-off value of 53 as the closest value at the intersection of the HRP and HRP density distributions (**Fig. 5d**). Using the above optimized criteria we show that

tnbcHRDscar increased the accuracy of classifying the HRD and HRP samples from 0.92 to 0.94 (**Fig. 5d**).

To test whether HR-status classification by tnbcHRDscar can predict clinical outcomes in TNBC, we next associated tnbcHRDscar with PFS in the TCGA cohort, and with distant relapse-free interval (DRFI) in an independent TNBC SNP-array dataset[20]. Patients with tnbcHRDscar-positive tumors had a significantly longer PFS as compared to those with tnbcHRDscar-negative tumors (log-rank p=0.014; **Fig. 5g**), while *BRCA*mut/del status or the Telli2016 algorithm did not associate with PFS (**Fig. 5e, f**). Consistently, only tnbcHRDscar showed a statistically significant association with DRFI (log-rank p=0.0022; **Fig. 5j**) in the independent validation set (**Fig. 5h to j**). Further, tnbcHRDscar classification in TCGA samples was also associated with OS (log-rank p=0.039; **Supplementary Fig. 5e**) similarly to the Telli2016 algorithm (log-rank p=0.039; **Supplementary Fig. 5d**). Additionally, we compared the performance of tnbcHRDscar with HRDetect[21], a predictor trained using WGS, to predict DRFI outcomes in the validation dataset. Interesting, HR-status classification by tnbcHRDscar showed a more significant association with DRFI (log-rank p=0.0021; **Supplementary Fig. 5g**) than HRDetect-high/low status (log-rank p=0.011; **Supplementary Fig. 5f**), regardless of the cut-off values selected for HRDetect (**Supplementary Fig. 5h**).

DISCUSSION

HRD tumors exhibit a distinct clinical phenotype with superior responses to platinum-based chemotherapy and sensitivity to PARP inhibitors. However, the accurate detection of HRD via somatic AIs has been confounded by lack of systematic approaches and analyses performed in admixtures of tumor types with distinct genomic drivers. Herein, we established HRDscar, a systematically optimized approach for HRD detection to improve patient selection and clinical outcomes in cancer.

Several genomic approaches have been utilized to detect HRD, including 1) identification of single genetic mutations leading to predicted HRD[22], 2) profiles of DNA repair deficiency gene expression[23,24], 3) specific mutational patterns accumulated due to HRD[8,9,25] or 4) structural genomic imbalances[7,26]. These genomic features have been implemented either alone, or in combinations in the search for optimal HRD detection which has profound therapeutic implications[27]. It is now becoming accepted that benefits from HR-directed therapy such as PARP inhibitors extend beyond the identification of HRD via individual genetic mutations[28]. This is due to the fact that genes such as *BRCA1/2* and *RAD51* paralogs can be altered beyond mutations, via e.g. hypermethylation or gene deletions[3,29], and not all genomic events leading to HRD have yet been defined[30]. Allelic imbalances are indicative of the genetic consequences of HRD and, although not dynamically reflective of tumors' functional HRD status, have shown promise as a biomarker predictive for the magnitude of benefit from PARP inhibitors, especially in the front-line setting[31,32]. The HRD test used in ovarian cancer clinical trials was, however, optimized using breast cancer samples or a mixture of breast cancer and ovarian cancer samples using *BRCA1/2* mutation as the sole denominator of HRD, and *BRCA*wt status as HRP[8,9,10]. Importantly, also European Society of Medical Oncology indicated an urgent need to optimize the HRD test in HGSC to especially improve the identification of the HRP tumors[23]. Via a pan-cancer characterization of AIs, we discovered marked differences in the AI patterns of HGSC as compared to other cancer types, including TNBC, especially among the *BRCA*wt tumors. This prompted us to systematically identify the genomic footprints of HRD-AIs specific for HGSC using carefully annotated multi-omics data from TCGA and an iterative machine learning and statistical approach.

ovaHRDscar levels were concordant with tumor genetic mutations and copy number events predictive of HRD status both in the TCGA dataset, and in an external validation cohort (HERCULES). We found significantly lower levels of ovaHRDscar in tumors with *CCNE1* amplification, proposed as mutually exclusive with HRD and associated with poor clinical outcomes[33]. In line with a previous report[17], tumors with *CDK12* mutation showed overall low

levels of ovaHRDscar and thus should be considered HRP. Further, ovaHRDscar showed a higher concordance with mutational signature 3 as compared to the Telli2016 algorithm. Most importantly, ovaHRDscar can be applied to detect HRD in HGSC samples using WGS or SNP-arrays, making it an attractive biomarker also for the clinical setting.

A dichotomous thresholding of a predictive HRD biomarker is needed for therapeutic decision making. In Telli2016, the cutoff for the total number of events was derived from a mixture of breast and ovarian cancer samples[10]. More recently, Tacaya et al. set out to improve the HRD test by adjusting the cutoff value in ovarian cancer[17], however only *BRCA*mut status was used for separating HRD from HRP samples and the same genomic features of HRD-AIs were used as in Telli et al. In ovaHRDscar, after optimization of both the genomic footprints of HRD-AIs and the cutoff, we identified more samples as being HRP, and reliably separated HRD from HRP with improved accuracy as compared to previous algorithms. In survival analyses, our fully optimized ovaHRDscar outperformed the two previous algorithms, indicating that both the identification of the genomic footprints of HRD-AIs, and selection of the optimal cutoff are needed to improve HRD detection in HGSC.

HRD tumors are known to have superior responses to platinum-based chemotherapy and prolonged overall survival[34]. Consistently, ovaHRDscar improved the prediction of PFS and OS for platinum-based chemotherapy in the OVA-TCGA, also after excluding patients used in the training set, even though clinical outcomes were not used in the optimization. ovaHRDscar significantly predicted PFS and OS also among only the *BRCA*wt tumors. Importantly, ovaHRDscar improved the prediction of clinical outcomes in two independent patient cohorts, and in multivariable models after adjusting for clinical covariables, indicating that ovaHRDscar reliably captures the phenotypic clinical behavior of HRD HGSCs. Further, using a disease-specific and systematic approach in the classification of HR-status, we could improve the prediction of clinical outcomes also in TNBC, with tnbcHRDscar significantly predicting disease-free survival in the TCGA and in an independent dataset. However, none of the

clinical cohorts included patients treated prospectively with e.g. PARP inhibitors, and therefore prospective validation in larger patient series is warranted.

Finally, as HGSC is characterized by marked intratumor heterogeneity, we aimed to assess whether the anatomical site of tumor sampling or the exposure to chemotherapy affect HRD assessment. Our analysis of 98 samples collected from different anatomical sites and treatment phases indicated that ovaHRDscar levels remain similar in spatiotemporally distinct samples within each patient, including anatomically site-matched samples collected before and after neoadjuvant chemotherapy. ovaHRDscar can thus be reliably assessed during routine clinical practice also after neoadjuvant chemotherapy, given that the tumor purity remains higher than 30%. Interestingly, ovaHRDscar levels were also similar between treatment-naive and relapsed tumors, reflecting the nature of HRD-AIs as a historical consequence of HRD, rather than a dynamic read-out of functional HRD. Overall, inter-patient variation was higher than intra-patient variation, however in four out of 21 (19%) of patients the HRD category was dependent on the sampling site/time. The survival and genetic analyses indicated that ovarian or adnexal sites, followed by omentum, could be the preferred sites for HRD testing. This finding warrants future validation in larger cohorts.

In conclusion, HRDscar shows promise as a robust, clinically feasible assay for both outcome prediction and selection of patients for HR-directed therapies. With the fully documented, publicly available algorithms and optimization pipeline HRDscar can be applied to other tumor types and implemented clinically for optimized patient selection to improve outcomes of patients with cancer.

MATERIAL AND METHODS

Data set collection and classification

For PanCan samples, allele-specific copy number segments were obtained from the Genomics Data Commons (GDC) portal (https://portal.gdc.cancer.gov/). List of TNBC

samples was adopted from Lehmann et al[35]. For TNBC, samples were considered with *BRCA*mut if reported by Knijnenburg et al.[36] to contain a gene deletion, gene mutation or gene silencing of *BRCA*1 or *BRCA*2; while *BRCA*wt those with no reported alterations.

For OVA-TCGA analysis: allele-specific copy number segments, DNA methylation, gene-level CNV profiles and clinical information data was obtained from the GDC data portal. Genes were considered with a “strong signal of deletion” if reported as such (labeled by -2) by Taylor et al.[37] and with signal of deletion those reported in the GDC portal. Gene promoter hypermethylation was considered when the probes up to 1500bp downstream the transcription start site had an average beta value ≥0.75. The catalog of mc3 somatic mutations was obtained from the PanCanAtlas-GDC data portal (https://gdc.cancer.gov/about-data/publications/pancanatlas). Somatic mutations were classified according to the recommendations of the American College of Medical Genetics and Genomics[38] using the web-tool VarSome[39] only pathogenic somatic mutations were considered in the analysis. For germline mutations we selected those labeled as pathogenic and prioritized by Huang et al. 2018[40]. Genes were considered part of the HR pathway, or other associated pathways according to the Kyoto Encyclopedia of Genes and Genomes database[41]. Complementary clinical information was obtained from the PanCanAtlas-GDC data portal. For PCAWG: allele-specific copy number segments, mutational drivers and clinical information were obtained from the International Cancer Genome Consortium data portal (https://dcc.icgc.org/pcawg).

HRD-AI optimization

First, we annotated the OVA-TCGA samples as HRD and HRP according to the following criteria: for HRD samples, samples harboring somatic or germline mutations, promoter hypermethylation or strong signal of deletion of the genes *BRCA1*, *BRCA2*, *RAD51* paralogs (**Fig. 2a**). For HRP sample annotation we selected those with none of the HRD selecting criteria, plus available data for methylation, gene deletion, somatic mutations and no deletion of any HR gene (**Fig. 2a**). HRD and HRD annotation was used as ground truth in posterior

accuracy assessment analysis. Then, for the annotated samples we quantified HRD-AIs according to Marquard et al[42] under different criteria. The length range criteria (l_{min}, l_{max}) of the quantified LOH events were exhaustively optimized by evaluating the classification power of each pair of l_{min} and l_{max} parameters that increase the accuracy of classifying the HRD and HRP annotated samples. The quantification of LST events, defined by the parameters *s* (minimum AI length) and *m* (maximum distance between the AI events that comprise an LST event), was optimized in the same manner. Finally, we counted TAI events if they were larger than *k*, where the length *k* was optimized following the same approach. The classification power was evaluated using 1) one tailed Mann Whitney U test 2) decision trees (R package 'rpart') taking the abundance of the selected AIs as split-point, samples above the split-point were considered as HRD an below HRP, True positive rate (TPR) and True Negative Rate (TNR) was computed when compared against the ground true (Fig. 2b). For each type of HRD-AI, it was selected the set of parameters (e.g. {l_{min}, l_{max}}{*s*,*m*}, *k*) with the highest product of U test p-aasdasda (p) and balance accuracy ($BA = \frac{TPR+TNR}{2}$), the product was inferred with the formula: $-1 * \log 10(p) * BA$. The selected set of parameters were incorporated in ovaHRDscar.

Survival analysis

Survival plots, log-rank aa and cox regression models were performed with an R script using the package 'a and 'survival'. Data from patients treated with cisplatin or carboplatin was selected. For PCAWG, data from all patients was used (no treatment information available). Only data from primary samples (treatment-naive) were used. *BRCA*mut/del status included pathogenic mutations, germline mutations and gene deletions with a "strong signal of deletion" as described above. Residual tumor after surgery was categorized as present or absent. For indicated cox regressions, residual tumor status or patient age at diagnosis was used as a covariable. Progression free survival (PFS) and overall survival (OS) were defined as in Liu et

al 2018[43]. The CHROD signature HR-status classification for PCAWG samples was adopted from Nguyen et al 2020[19].

Prospective HERCULES and TERVA data analysis

The tumor samples were prospectively collected in the HERCULES (http://www.project-hercules.eu) and TERVA projects (https://www.healthcampusturku.fi/innovation-new/terva-project/). The Ethics Committee of the Hospital District of Southwest Finland, approved both studies ETMK Dnro: 145 /1801/2015. All patients gave their informed consent. For HERCULES, paired fresh tumor samples and blood normal samples were sequenced using Illumina-HiSeq X Ten WGS. Raw reads were trimmed and filtered with Trimmomatic[44] followed by duplicate marking with Picard Tools (https://broadinstitute.github.io/picard/). Alignment to the human genome GRCh38 was done using the burrows wheeler aligner BWA-MEM[45]. Mutations were detected using GATK4-Mutect2 approach[46]. Mutect2 was used for detection of allele specific copy numbers; regions listed in the ENCODE blacklist[47] were omitted. Calculation of tumor purity was estimated in two ways: 1) Based in somatic copy-number profiles using the software Ascat[48] 2) Based in *TP53* variant allele frequency (*TP53*-VAF), purity was estimated using the formula: *2 / ((CN / TP53-VAF) - (CN - 2)),* where CN corresponds to the copy-number value in the corresponding somatic mutations in *TP53*; subsequently the higher purity value was selected. For the TERVA samples tumor-only profiling, tumor samples were genotyped using the Infinium™ Global Screening Array-24 v2.0. B allele frequency and LogR ratios per sample probe was calculated using Illumina-GenomeStudio. Ascat software was used for the detection of allele specific copy numbers, *ascat.predictGermlineGenotypes* module was performed adjusting parameters according to a panel of 200 normal germline blood samples.

Statistics

The statistics analysis was performed in R. Difference in mean abundances was calculated using Mann Whitney U test. The distribution Skewness of AI sizes in different types of cancers

was performed using the package DescTools. Agreement was calculated using the Cohen kappa test. Concordance was measured using Lin's concordance correlation coefficient. Level of correlations was assessed using Pearson correlations. P value less than 0.05 was considered statistically significant.

Code Availability

The code used to perform the HRD-AI optimization is available on Github: (https://github.com/farkkilab/findHRD-AIs), ovaHRDscar implementation is available as and R package on Github (https://github.com/farkkilab/ovaHRDscar).

Data availability

Data available upon request.

ACKNOWLEDGMENTS

This study was funded by the Sigrid Jusélius Foundation (AF, LK), Finnish cancer society (AF, JC, LK), Academy of Finland (grant number 322979 to AF, grant numbers 314394 and 322178 to LK, grant number 314398 to SaHi), Paolo Foundation (AF), The Finnish Medical Foundation (AF), Finnish Cultural Foundation (AF), Instrumentarium Foundation (AF, JC), University of Helsinki (AF), AstraZeneca (to SaHi), the European Union's Horizon 2020 research and innovation program under grant agreement No 667403 for HERCULES (SHa, JH, SHi) and No 965193 for DECIDER (SHa, JH, SHi). We also wish to thank FIMM genomics core facility, The FINNPEC for the statistical reference data, Johan Staaf for assistance in TNBC data access, and the IT Center for Science (CSC) for computational resources.

COMPETING INTEREST

The authors declare no competing interests

Supplementary Information is available for this paper

REFERENCES

1 Ceccaldi, R., Rondinelli, B. & D'Andrea, A. D. Repair Pathway Choices and Consequences at the Double-Strand Break. *Trends Cell Biol* **26**, 52-64, doi:10.1016/j.tcb.2015.07.009 (2016).

2 Lord, C. J. & Ashworth, A. PARP inhibitors: Synthetic lethality in the clinic. *Science* **355**, 1152-1158, doi:10.1126/science.aam7344 (2017).

3 Torre, L. A. *et al.* Ovarian cancer statistics, 2018. *CA Cancer J Clin* **68**, 284-296, doi:10.3322/caac.21456 (2018).

4 Konstantinopoulos, P. A., Ceccaldi, R., Shapiro, G. I. & D'Andrea, A. D. Homologous Recombination Deficiency: Exploiting the Fundamental Vulnerability of Ovarian Cancer. *Cancer Discov* **5**, 1137-1154, doi:10.1158/2159-8290.CD-15-0714 (2015).

5 Ray-Coquard, I. *et al.* Olaparib plus Bevacizumab as First-Line Maintenance in Ovarian Cancer. *N Engl J Med* **381**, 2416-2428, doi:10.1056/NEJMoa1911361 (2019).

6 Gonzalez-Martin, A. *et al.* Niraparib in Patients with Newly Diagnosed Advanced Ovarian Cancer. *N Engl J Med* **381**, 2391-2402, doi:10.1056/NEJMoa1910962 (2019).

7 Popova, T. *et al.* Ploidy and large-scale genomic instability consistently identify basal-like breast carcinomas with BRCA1/2 inactivation. *Cancer Res* **72**, 5454-5462, doi:10.1158/0008-5472.CAN-12-1470 (2012).

8 Abkevich, V. *et al.* Patterns of genomic loss of heterozygosity predict homologous recombination repair defects in epithelial ovarian cancer. *Br J Cancer* **107**, 1776-1782, doi:10.1038/bjc.2012.451 (2012).

9 Birkbak, N. J. *et al.* Telomeric allelic imbalance indicates defective DNA repair and sensitivity to DNA-damaging agents. *Cancer Discov* **2**, 366-375, doi:10.1158/2159-8290.CD-11-0206 (2012).

10 Telli, M. L. *et al.* Homologous Recombination Deficiency (HRD) Score Predicts Response to Platinum-Containing Neoadjuvant Chemotherapy in Patients with Triple-

Negative Breast Cancer. *Clin Cancer Res* **22**, 3764-3773, doi:10.1158/1078-0432.CCR-15-2477 (2016).

11 Stefansson, O. A. *et al.* Genomic profiling of breast tumours in relation to BRCA abnormalities and phenotypes. *Breast Cancer Res* **11**, R47, doi:10.1186/bcr2334 (2009).

12 Breiman, L. *Classification and regression trees*. (Wadsworth International Group, 1984).

13 Consortium, I. T. P.-C. A. o. W. G. Pan-cancer analysis of whole genomes. *Nature* **578**, 82-93, doi:10.1038/s41586-020-1969-6 (2020).

14 de Luca, X. M. *et al.* Using whole-genome sequencing data to derive the homologous recombination deficiency scores. *NPJ Breast Cancer* **6**, 33, doi:10.1038/s41523-020-0172-0 (2020).

15 Alexandrov, L. B. *et al.* The repertoire of mutational signatures in human cancer. *Nature* **578**, 94-101, doi:10.1038/s41586-020-1943-3 (2020).

16 Gulhan, D. C., Lee, J. J., Melloni, G. E. M., Cortes-Ciriano, I. & Park, P. J. Detecting the mutational signature of homologous recombination deficiency in clinical samples. *Nat Genet* **51**, 912-919, doi:10.1038/s41588-019-0390-2 (2019).

17 Takaya, H., Nakai, H., Takamatsu, S., Mandai, M. & Matsumura, N. Homologous recombination deficiency status-based classification of high-grade serous ovarian carcinoma. *Sci Rep* **10**, 2757, doi:10.1038/s41598-020-59671-3 (2020).

18 Polterauer, S. *et al.* Prognostic value of residual tumor size in patients with epithelial ovarian cancer FIGO stages IIA-IV: analysis of the OVCAD data. *Int J Gynecol Cancer* **22**, 380-385, doi:10.1097/IGC.0b013e31823de6ae (2012).

19 Nguyen, L., J, W. M. M., Van Hoeck, A. & Cuppen, E. Pan-cancer landscape of homologous recombination deficiency. *Nat Commun* **11**, 5584, doi:10.1038/s41467-020-19406-4 (2020).

20 Staaf, J. *et al.* Whole-genome sequencing of triple-negative breast cancers in a population-based clinical study. *Nat Med* **25**, 1526-1533, doi:10.1038/s41591-019-0582-4 (2019).

21 Davies, H. *et al.* HRDetect is a predictor of BRCA1 and BRCA2 deficiency based on mutational signatures. *Nat Med* **23**, 517-525, doi:10.1038/nm.4292 (2017).

22 Wagle, N. *et al.* High-throughput detection of actionable genomic alterations in clinical tumor samples by targeted, massively parallel sequencing. *Cancer Discov* **2**, 82-93, doi:10.1158/2159-8290.CD-11-0184 (2012).

23 Kang, J., D'Andrea, A. D. & Kozono, D. A DNA repair pathway-focused score for prediction of outcomes in ovarian cancer treated with platinum-based chemotherapy. *J Natl Cancer Inst* **104**, 670-681, doi:10.1093/jnci/djs177 (2012).

24 Konstantinopoulos, P. A. *et al.* Gene expression profile of BRCAness that correlates with responsiveness to chemotherapy and with outcome in patients with epithelial ovarian cancer. *J Clin Oncol* **28**, 3555-3561, doi:10.1200/JCO.2009.27.5719 (2010).

25 Wang, Y. K. *et al.* Genomic consequences of aberrant DNA repair mechanisms stratify ovarian cancer histotypes. *Nat Genet* **49**, 856-865, doi:10.1038/ng.3849 (2017).

26 Polak, P. *et al.* A mutational signature reveals alterations underlying deficient homologous recombination repair in breast cancer. *Nat Genet* **49**, 1476-1486, doi:10.1038/ng.3934 (2017).

27 Swisher, E. M. *et al.* Rucaparib in relapsed, platinum-sensitive high-grade ovarian carcinoma (ARIEL2 Part 1): an international, multicentre, open-label, phase 2 trial. *Lancet Oncol* **18**, 75-87, doi:10.1016/S1470-2045(16)30559-9 (2017).

28 Miller, R. E. *et al.* ESMO recommendations on predictive biomarker testing for homologous recombination deficiency and PARP inhibitor benefit in ovarian cancer. *Ann Oncol* **31**, 1606-1622, doi:10.1016/j.annonc.2020.08.2102 (2020).

29 Golmard, L. *et al.* Contribution of germline deleterious variants in the RAD51 paralogs to breast and ovarian cancers. *Eur J Hum Genet* **25**, 1345-1353, doi:10.1038/s41431-017-0021-2 (2017).

30 Radhakrishnan, S. K., Jette, N. & Lees-Miller, S. P. Non-homologous end joining: emerging themes and unanswered questions. *DNA Repair (Amst)* **17**, 2-8, doi:10.1016/j.dnarep.2014.01.009 (2014).

31 Ray-Coquard, I. *et al.* Olaparib plus Bevacizumab as First-Line Maintenance in Ovarian Cancer. *N Engl J Med* **381**, 2416-2428, doi:10.1056/NEJMoa1911361 (2019).

32 Gonzalez-Martin, A. *et al.* Niraparib in Patients with Newly Diagnosed Advanced Ovarian Cancer. *N Engl J Med* **381**, 2391-2402, doi:10.1056/NEJMoa1910962 (2019).

33 Etemadmoghadam, D. *et al.* Synthetic lethality between CCNE1 amplification and loss of BRCA1. *Proc Natl Acad Sci U S A* **110**, 19489-19494, doi:10.1073/pnas.1314302110 (2013).

34 Norquist, B. M. *et al.* Mutations in Homologous Recombination Genes and Outcomes in Ovarian Carcinoma Patients in GOG 218: An NRG Oncology/Gynecologic Oncology Group Study. *Clin Cancer Res* **24**, 777-783, doi:10.1158/1078-0432.CCR-17-1327 (2018).

35 Lehmann, B. D. *et al.* Refinement of Triple-Negative Breast Cancer Molecular Subtypes: Implications for Neoadjuvant Chemotherapy Selection. *PLoS One* **11**, e0157368, doi:10.1371/journal.pone.0157368 (2016).

36 Knijnenburg, T. A. *et al.* Genomic and Molecular Landscape of DNA Damage Repair Deficiency across The Cancer Genome Atlas. *Cell Rep* **23**, 239-254 e236, doi:10.1016/j.celrep.2018.03.076 (2018).

37 Taylor, A. M. *et al.* Genomic and Functional Approaches to Understanding Cancer Aneuploidy. *Cancer Cell* **33**, 676-689 e673, doi:10.1016/j.ccell.2018.03.007 (2018).

38 Richards, S. *et al.* Standards and guidelines for the interpretation of sequence variants: a joint consensus recommendation of the American College of Medical Genetics and Genomics and the Association for Molecular Pathology. *Genet Med* **17**, 405-424, doi:10.1038/gim.2015.30 (2015).

39 Kopanos, C. *et al.* VarSome: the human genomic variant search engine. *Bioinformatics* **35**, 1978-1980, doi:10.1093/bioinformatics/bty897 (2019).

40 Huang, K. L. *et al.* Pathogenic Germline Variants in 10,389 Adult Cancers. *Cell* **173**, 355-370 e314, doi:10.1016/j.cell.2018.03.039 (2018).

41 Kanehisa, M. & Goto, S. KEGG: kyoto encyclopedia of genes and genomes. *Nucleic Acids Res* **28**, 27-30, doi:10.1093/nar/28.1.27 (2000).

42 Marquard, A. M. *et al.* Pan-cancer analysis of genomic scar signatures associated with homologous recombination deficiency suggests novel indications for existing cancer drugs. *Biomark Res* **3**, 9, doi:10.1186/s40364-015-0033-4 (2015).

43 Liu, J. *et al.* An Integrated TCGA Pan-Cancer Clinical Data Resource to Drive High-Quality Survival Outcome Analytics. *Cell* **173**, 400-416 e411, doi:10.1016/j.cell.2018.02.052 (2018).

44 Bolger, A. M., Lohse, M. & Usadel, B. Trimmomatic: a flexible trimmer for Illumina sequence data. *Bioinformatics* **30**, 2114-2120, doi:10.1093/bioinformatics/btu170 (2014).

45 Li, H. & Durbin, R. Fast and accurate short read alignment with Burrows-Wheeler transform. *Bioinformatics* **25**, 1754-1760, doi:10.1093/bioinformatics/btp324 (2009).

46 Cibulskis, K. *et al.* Sensitive detection of somatic point mutations in impure and heterogeneous cancer samples. *Nat Biotechnol* **31**, 213-219, doi:10.1038/nbt.2514 (2013).

47 Amemiya, H. M., Kundaje, A. & Boyle, A. P. The ENCODE Blacklist: Identification of Problematic Regions of the Genome. *Sci Rep* **9**, 9354, doi:10.1038/s41598-019-45839-z (2019).

48 Van Loo, P. *et al.* Allele-specific copy number analysis of tumors. *Proc Natl Acad Sci U S A* **107**, 16910-16915, doi:10.1073/pnas.1009843107 (2010).

FIGURE LEGENDS

Figure 1. Pan-cancer characterization of AIs reveal unique patterns in HGSC. a Types of cancer with more than 200 samples in TCGA, their corresponding number of samples are shown in green the bars. **b** Number of AIs bigger than 3Mb and smaller than 50Mb per sample,

HGSC shows the highest abundance of AIs. **c** Median length of AIs (bigger than 3Mb and smaller than 50Mb) per sample, HGSC shows the lowest median size per sample. **d** Hierarchical clustering for the types of cancer using as variables the median length, median number of AIs per sample and the skewness of the distribution of AIs sizes. **e** In total HGSC samples show no higher (U test) amount of AIs than TNBC. **f** Comparison of *BRCA*mut samples (somatic deletion, promoter hypermethylation and gene deletions of *BRCA*1/2 genes), shows no significantly higher amounts (U test) of AIs in HGSC than in TNBC. **g** Comparison of *BRCA*wt samples, shows higher amounts of AIs in HGSC than in TNBC (U test, p=0.002). **h** Difference in abundance for AIs of specific sizes between HGSC and TNBC, dot sizes correspond to U test p-values and dot colors to the fold change (ratio of HGSC-TNBC abundance of AIs minus one), only dots for corresponding significantly differences are shown (U test, $p < 0.05$).

Figure 2. Optimization of size selection for AIs associated with HRD in HGSC and relationship with HRD biomarkers. a Selection criteria for annotating HRD, HRP and Undefined HGSC samples in OVA-TCGA. **b** A schematic of the approach used to optimize the criteria for selecting HRD-AIs in HGSC samples. Exhaustively were taken HRD-AIs under different criteria (see methods), for each tested criteria it was evaluated: 1) the difference of abundance (U test) of the selected HRD-AIs between HRD versus HRP samples, 2) the HR-status classification accuracy of a decision tree; the criteria with highest accuracy and U test significance was selected for ovaHRDscar. **c** For LST event optimization, the size of dots represent the decision tree balanced accuracy (BA) of classifying HRD and HRP when selecting AIs of the corresponding criteria, dot colors correspond to the statistical (U test, p value) difference in abundance of AIs between HRD versus HRP samples. Black box corresponds to the selection criteria proposed by Telli2016, blue box correspond to the best BA and U test value. **d** Evaluation of ovaHRDscar values as a cut-off to define HR-status (samples with bigger or equal values considered as HRD), black dots correspond to the

balanced accuracy (BA) of the classification of the annotated HRD and HRP samples using the given cut-off value, confidence intervals are shown in grey, value of 54 (red dashed line) correspond to the highest BA. **e** Density distribution of HRD-AIs according to Telli2016 and ovaHRDscar algorithms. The red dashed line represents the cutoff established to define HR-status for Telli2016 (>= 42) and for ovaHRDscar (>= 54), BA of classifying the annotated HRD and HRP is shown. **f** Levels of ovaHRDscar in OVA-TCGA samples harboring different genetic or epigenetic alterations associated with HRD in HGSC[4]. In the outer ring of the pie chart every line represents a sample; in the center of the pie chart the colors correspond to the average number of HRD-AIs per genetic or epigenetic alteration. Somatic mutations (somaticmut) included gene deletions. **g** The proportion of single base substitution signature 3 (SBS3) is correlated (Pearson r'=0.38) with the number of ovaHRDscar in PCAWG samples. **h** The SBS3 status inferred by SigMA[16] has a higher agreement with ovaHRDscar (agreement=78.3%, cohen's kappa = 0.56) than with the Telli2016 algorithm (agreement=68.5%, cohen's kappa = 0.32), in the pie charts and table + and - correspond respectively to the number of HRD positive and HRD negative samples identified under each criterion. In the button is shown the number of samples selected under the corresponding criterion and the level of agreement.

Figure 3. HRD detected by ovaHRDscar is associated with higher PFS and OS in HGSC patients treated with platinum. a to c Kaplan-Meier plots of PFS in OVA-TCGA patients stratified with different criteria, in **a** patients were stratified according to *BRCA*mut/del status with no significant difference in their PFS probability over time (log-rank, p=0.78); in **b** patients were stratified according to Telli2016 algorithm (log-rank, p=0.017); in **c** patients were stratified using the ovaHRDscar algorithm, HRD patients had a improvement in PFS time over HRP (log-rank, p=4.4e-04). **d** Cox regression results for the association of PFS with several genomic HR-status classification criteria (*BRCA*mut/del, Telli2016, Tacaya2020, ovaHRDscar) in two independent cohorts, for every regression it was used as covariable the residual tumor status (yes or no) after surgery. Three panels are shown: at left the OVA-TCGA

cohort, at the middle OVA-TCGA cohort excluding the annotated HRD and HRP samples used for the HRD-AIs optimization, at the right the HERCULES WGS prospective cohort. Inside each panel is shown for classification criteria: the number of patients (N) selected as positive or HRD and their corresponding proportion (Prop), the hazard-ratio (HR) for the cox regression and the p-value (Pval) of the regression. ovaHRDscars show higher significance (lower p values) in every cohort, even after excluding patients with tumors harboring *BRCA*mut/del (bottom section). **e to g,** Kaplan-Meier plots of OS for OVA-TCGA patients selected using different criteria, ovaHRDscar show the higher significance (lower long-rank test p-values). **h** Cox regression results for the association of OS with several genomic HR-status classification criteria (*BRCA*mut/del, Telli2016, Tacaya2020, ovaHRDscar) in two independent cohorts. Panel at the right corresponds to the PCAWG samples, the left and center panels and their corresponding columns correspond to those described in panel d. ovaHRDscars show higher significance (lower p values) in every cohort, even after excluding patients with tumors harboring *BRCA*mut/del (bottom section).

Figure 4. Low intra-patient anatomical variation of ovaHRDscar. a Overview of the samples and their corresponding ovaHRDscar levels per patient within a prospective cohort analyzed by WGS (HERCULES). Per patient tumor samples were taken in three different treatment times and from different anatomical sites as described; in parentheses are displayed the corresponding number of samples. **b** Levels of ovaHRDscar in samples harboring different genetic or epigenetic alterations associated with HRD, in the outer ring of the pie chart every bar represents a sample carrying the corresponding alteration; in the center of the pie chart the colors correspond to the average levels of ovaHRDscar per alteration. **c** ovaHRDscar values between paired samples for each patient (connected dots) does not vary significantly (paired U test) over treatment phase. **d** Cox regression results for the association of PFS with HR-status classification by Telli2016 and ovaHRDscar, the HR-status per patient was assessed using three anatomical sample prioritization approaches: 1) average HRD-AIs per all samples 2) omentum, and OVA/ADN if omentum sample not available (OME-OVA/ADN)

3) OVA/ADN, and then omentum if OVA/ADN not available (OVA/ADN-OME). Last prioritization approach has a higher association with PFS.

Figure 5. Optimization of HRD-AI in TNBC improves the prediction of clinical outcomes. **a** Number of AIs for TNBCs HRD and HRP samples in TCGA. **b** Optimization for LOH events, size of dots represent the decision tree balanced accuracy (BA) of classifying HRD and HRP when selecting LOH the corresponding size, dot colors correspond to the statistical (U test, p value) difference in abundance of LOH between HRD versus HRP samples. Black box corresponds to the selection criteria proposed by Telli2016, blue box correspond to the best BA and U test value. **c** Evaluation of tnbcHRDscar values as a cut-off to define HR-status (samples with bigger or equal values considered as HRD), black dots correspond to the balanced accuracy (BA) of the classification of the HRD and HRP samples using the given cut-off value, confidence intervals are shown in grey, value of 53 (red dashed line) selected with highest BA. **d** Density distribution of HRD-AIs according to Telli2016 and tnbcHRDscar algorithms. The red dashed line represents the cutoff established to define HR-status for Telli2016 (>= 42) and for tnbcHRDscar (>= 53). The balanced accuracy (BA) for classifying the HR-status is shown for Telli2016 and ovaHRDscar algorithm. **e to g** Kaplan-Meier plots of PFS for TNBC patients in TCGA stratified with different criteria, in **e** patients were stratified according to *BRCA*mut/del status with no significant difference in their PFS probability over time (log-rank, p=0.48); in **f** patients stratified according to Telli2016 algorithm (log-rank, p=0.082); in **g** patients stratified using the tnbcHRDscar algorithm (log-rank, p=0.014). **h to j** Kaplan-Meier plots of distant relapse-free interval (DRFI) for TNBC patients in validation set stratified with different criteria, in **h** patients were stratified according to *BRCA*mut/del status with no significant difference in their DRFI probability over time (log-rank, p=0.95); in **i** patients stratified according to Telli2016 algorithm (log-rank, p=0.13); in **j** patients stratified using the tnbcHRDscar algorithm (log-rank, p=0.0022).

SUPPLEMENTARY FIGURE LEGENDS

Supplementary Figure 1. Pan-cancer characterization of LOH and unique patterns in HGSC. a. Boxplot for the number of LOH bigger than 3Mb and smaller than 50Mb per sample, HGSC shows the higher abundance of LOH. **b** Median length of LOH (bigger than 3Mb and smaller than 50Mb) per sample. **c** Hierarchical clustering of the types of cancer using as variables the median length, median number of LOH per sample and the skewness of the distribution of LOH sizes. **d** HGSC samples show a lower amount of LOH than TNBC (U test, p=0.005). **e** Comparison of *BRCA*mut samples (somatic deletion, promoter hypermethylation and gene deletions of *BRCA*1/2 genes), HGSC shows higher amounts of LOH than TNBC (U test, p=0.021). **f** Comparison of *BRCA*wt samples, not statistical significant abundance difference of LOH (U test, NS) between HGSC and TNBC.

Supplementary Figure 2. Descriptive statistics of HRD and HRP in HGSC and optimization of HRD selection. a Number of allelic imbalances in HRD and HRP samples in OVA-TCGA, in average HRD samples contain a higher number of allelic imbalances (U test, p value=0.0028). **b** The average proportion of segments (AI or normal) equal or greater than the given size in HRD (red) and HRP (blue) samples, the blue and red lines correspond to smoothing using cubic splines, confidence intervals are shown in shaded colors. **c** Density distribution of LOH events in HRD (red) and HRP (blue) samples. **d** LOH specific AIs size cutoffs (blue boxes) outperform those reported by Telli et al. 2016 (black box); the size of dots represent the decision tree balanced accuracy (BA) when using the corresponding cutoff, colors correspond to the statistical (U test p value) difference in abundance of AIs between HRD versus HRP samples. **e** Statistical significance for identifying HRD samples using three tandem allelic imbalances LSTs of a given minimum size (x axis) and distance between them smaller than 1 to 4 Mb (y axis). Dot sizes and colors resemble those in Supplementary Figure

1e. **f** The selection of TAIs >1Mb (red dashed line) differentiate HRD from HRP samples better than using all TAIs, the upper panel shows statistical (U test, p values) difference in abundance of AIs between HRD versus HRP samples when selecting the corresponding TAIs, dot sizes and colors in the lower panel correspond to the description in panel d and e. **g** ovaHRDscar levels per genomic alteration in OVA-TCGA, U test p values are shown for the comparison of levels between the corresponding alterations versus CCNE1 amplification. **h** Bland-Altman plot that shows the concordance (Concordance correlation coefficient, *CCC* = 0.90) between the number of ovaHRDscars detected by SNP-arrays and WGS in the intersecting samples from OVA-TCGA and PCAWG. **i** Correlation (Pearson, r=0.38) between the SBS3 proportion in WGS data from PCAWG versus the number of scars using the Telli2016 approach.

Supplementary Figure 3. HRD detected by ovaHRDscar is associated with better PFS and OS in HGSC patients after normalizing with relevant covariables. a to c Kaplan-Meier plots of PFS in HERCULES cohort, the patients were stratified using different criteria; in the left panel (**a**) patients were stratified according to *BRCA*mut/del status with no significant difference in their PFS probability (p=0.15); in the middle panel (**b**) patients were stratified according to Telli2016 algorithm; in the right panel (**c**) patients were stratified using the ovaHRDscar algorithm and there is a significant difference (improvement) in PFS time (p = 0.001). **d** Hazard ratios (HR) for improvement of PFS in HGSC patients using different criteria in two independent cohorts, the colors, rows and columns descriptions are the same as in Figure 2d. **e to f** Kaplan-Meier plots of PFS in the TERVA cohort, patients were stratified using different criteria; in the left panel (**e**) patients were stratified according to Telli2016 algorithm; in the right panel (**f**) samples were stratified using the ovaHRDscar. **g** Hazard ratios (HR) for improvement of PFS in the TERVA cohort, patients were stratified using different criteria the colors, rows and columns descriptions are the same as in Figure 2b. **h to j** Kaplan-Meier plots of OS in HERCULES patients and stratified using different criteria; in the left panel (**h**) patients were stratified according to *BRCA*mut/del status with no significant difference (p=0.045), in the middle panel (**i**) patients were stratified according to Telli2016 algorithm with no significant

difference (p=0.022), in the right panel (**j**) samples were stratified using the ovaHRDscar algorithm and there is a significant difference (improvement) in PFS time (p = 0.006). **k** Hazard ratios (HR) for improvement of OS in HGSC, patients were stratified using different criteria inside two independent cohorts, for every cox regression it was used as covariable the patient age at diagnosis, the rows, colors and columns descriptions are the same as in Figure 2h. **l to m** Kaplan-Meier plots of OS in the PCAWG cohort, at the left panel (**l**) the patients were stratified according to CHORD signature reported by developers, at the right panel (**m**) the patients were stratified according to ovaHRDscar approach. **n** Hazard ratios (HR) for improvement of OS in the PCAWG cohort, patients were stratified using different CHROD and ovaHRDscar criteria; the dot colors, rows and columns descriptions are the same as in Figure 2d.

Supplementary Figure 4. Differences in ovaHRDcar within-patient, and relationship with tumor purity. **a** Difference in the ovaHRDscar values intra-patients and inter-patients in the HERCULES prospective cohort (U test, p=1.95e-38)**.** **b** Schematic of paired specimens sampled over treatment time, with tumor purity and ovaHRDscar levels indicated. **c** For each patient we calculated the difference in ovaHRDscar and purity between every pair of their samples, no association between purity and ovaHRDscar difference (Pearson, p=0.4), patient P4 was ignored in the analysis because it is an outlier. **d** HR-status classification using five different approaches to assess the ovaHRDscar values per patient (see results sections), per patient genomic alterations related with HR are shown. **e** Hazard ratios (HR) for improvement of PFS in the HERCULES cohort using different criteria to determine HR and under the five different approaches to assess the scar values (see results sections), for every cox regression it was used as covariable the residual tumor status (yes or no) after surgery. Colors, rows and column descriptions are the same as in Figure 2b.

Supplementary Figure 5. Optimization of HRD-AI in TNBC improves the prediction of clinical outcomes. **a** Optimization of LST events, size of dots represent the decision tree

balanced accuracy (BA) of classifying HRD and HRP when selecting LSTs with the corresponding criteria, dot colors correspond to the statistical (U test, p value) difference in abundance of the selected LSTs between HRD versus HRP samples. Black box corresponds to the selection criteria proposed by Telli2016, blue box correspond to the best BA and U test value. **b** The selection of TAIs >1Mb (red dashed line) differentiate HRD from HRP samples better than using all TAIs, the upper panel shows statistical (U test, p values) difference in abundance of AIs between HRD versus HRP samples when selecting the corresponding TAIs, dot sizes and colors in the lower panel correspond to the description in panel a. **c to e** Kaplan-Meier plots of OS for TNBC patients in TCGA stratified with different criteria, in **c** patients were stratified according to *BRCA*mut/del status (log-rank, p=0.057); in **d** patients were stratified according to Telli2016 algorithm (log-rank, p=0.039); in **e** patients stratified using the tnbcHRDscar algorithm (log-rank, p=0.039). **f to g** Kaplan-Meier plots of distant relapse-free interval (DRFI) for TNBC patients in validation set stratified with different criteria, in **f** patients were stratified according to HRDetect-high/low status with (log-rank, p=0.011); in **g** patients were stratified according to tnbcHRDscar algorithm (log-rank, p=0.0021). **h** Selection of different values to define HRDetect-high/low status for patient stratification of the TNBC in validation set and its association with DRFI (Log-rank test, p-value), patients with intermediate HRDetect values were ignored. In blue line, the Log-rank p-value when using tnbcHRDscar.

Figure 1

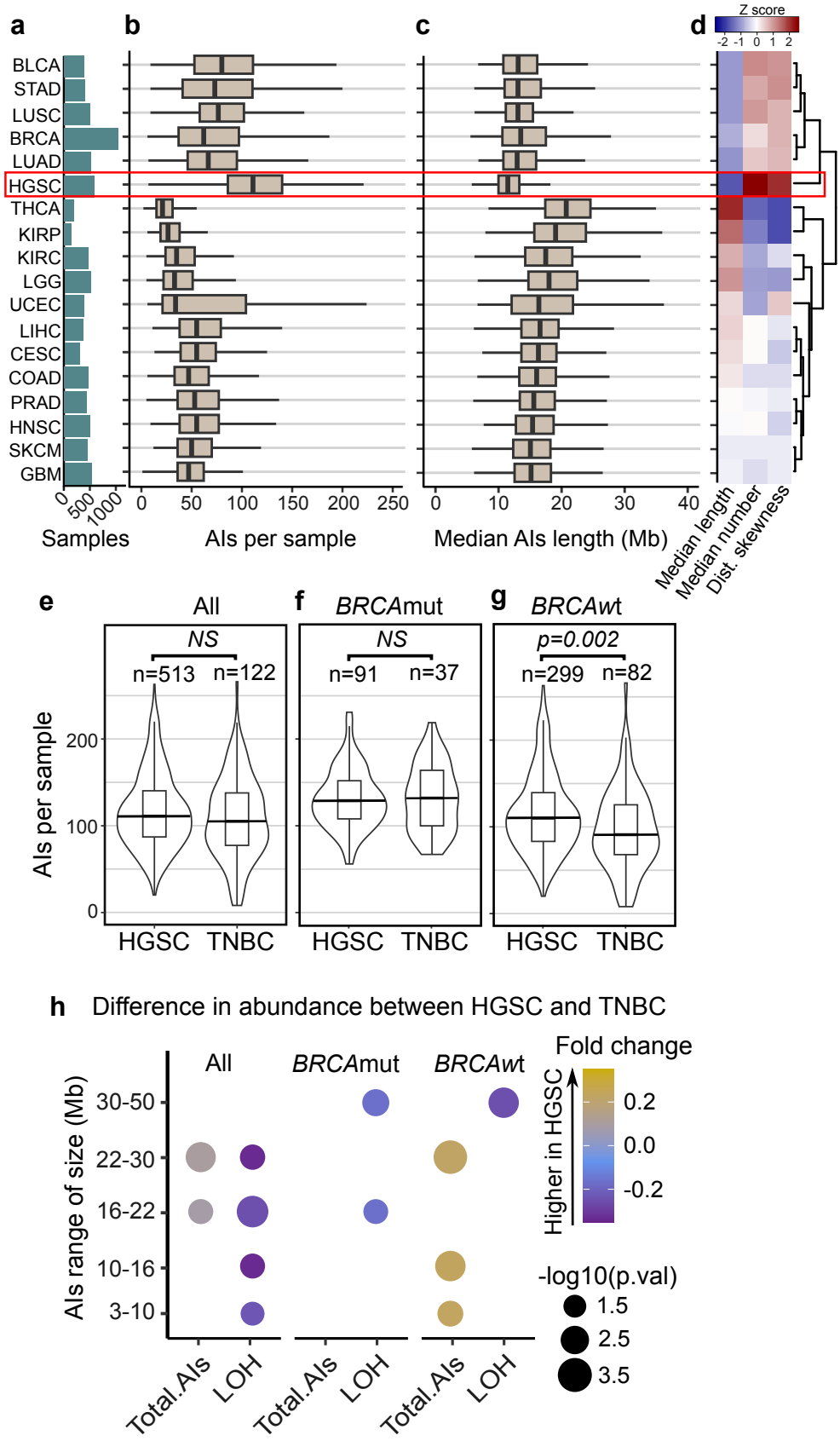
a
b
c
d
Z score
-2 -1 0 1 2
BLCA
STAD
LUSC
BRCA
LUAD
HGSC
THCA
KIRP
KIRC
LGG
UCEC
LIHC
CESC
COAD
PRAD
HNSC
SKCM
GBM
0 500 1000
Samples
0 50 100 150 200 250
AIs per sample
0 10 20 30 40
Median AIs length (Mb)
Median length
Median number
Dist. skewness
e
All
NS
n=513 n=122
f
BRCAmut
NS
n=91 n=37
g
BRCAwt
p=0.002
n=299 n=82
AIs per sample
0 100 200
HGSC TNBC
HGSC TNBC
HGSC TNBC
h Difference in abundance between HGSC and TNBC
All
BRCAmut
BRCAwt
AIs range of size (Mb)
30-50
22-30
16-22
10-16
3-10
Total.AIs LOH
Total.AIs LOH
Total.AIs LOH
Fold change
Higher in HGSC
0.2
0.0
-0.2
-log10(p.val)
1.5
2.5
3.5

Figure 2

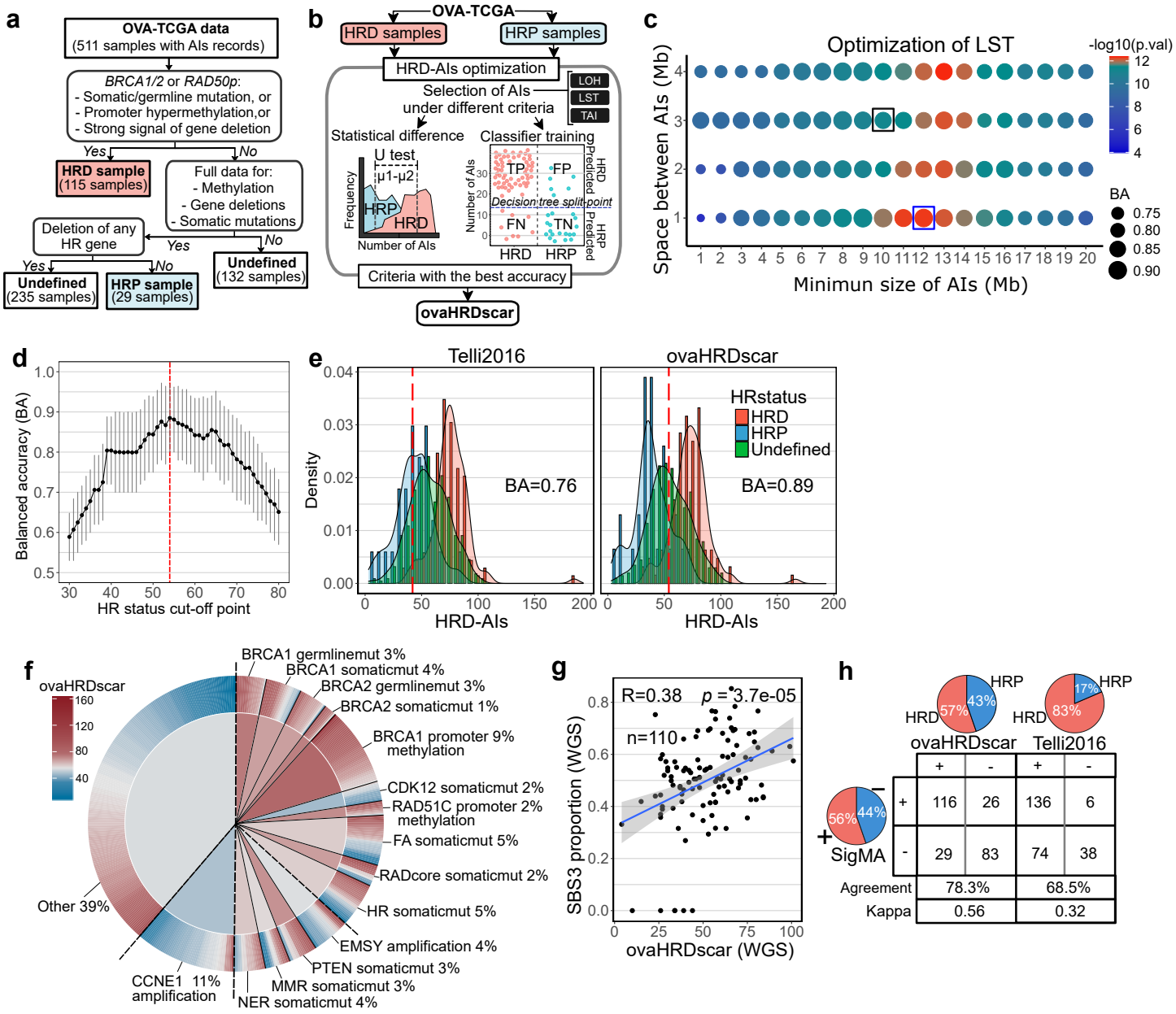

a
OVA-TCGA data
(511 samples with AIs records)
BRCA1/2 or RAD50p:
- Somatic/germline mutation, or
- Promoter hypermethylation,or
- Strong signal of gene deletion
Yes
No
HRD sample
(115 samples)
Full data for:
- Methylation
- Gene deletions
- Somatic mutations
Deletion of any HR gene
Yes
No
Undefined
(132 samples)
Yes
No
Undefined
(235 samples)
HRP sample
(29 samples)
b
OVA-TCGA
HRD samples
HRP samples
HRD-AIs optimization
Selection of AIs under different criteria
LOH
LST
TAI
Statistical difference
Classifier training
U test
μ1-μ2
Frequency
HRP
HRD
Number of AIs
Number of AIs
TP
FP
FN
TN
Decision tree split-point
HRD Predicted
HRP Predicted
HRD
HRP
Criteria with the best accuracy
ovaHRDscar
c
Optimization of LST
-log10(p.val)
Space between AIs (Mb)
Minimun size of AIs (Mb)
BA
0.75
0.80
0.85
0.90
d
Balanced accuracy (BA)
HR status cut-off point
e
Telli2016
ovaHRDscar
Density
HRstatus
HRD
HRP
Undefined
BA=0.76
BA=0.89
HRD-AIs
HRD-AIs
f
ovaHRDscar
BRCA1 germlinemut 3%
BRCA1 somaticmut 4%
BRCA2 germlinemut 3%
BRCA2 somaticmut 1%
BRCA1 promoter 9% methylation
CDK12 somaticmut 2%
RAD51C promoter 2% methylation
FA somaticmut 5%
RADcore somaticmut 2%
HR somaticmut 5%
EMSY amplification 4%
PTEN somaticmut 3%
MMR somaticmut 3%
NER somaticmut 4%
CCNE1 11% amplification
Other 39%
g
R=0.38
p = 3.7e-05
n=110
SBS3 proportion (WGS)
ovaHRDscar (WGS)
h
HRP
HRD
57%
43%
ovaHRDscar
HRP
HRD
83%
17%
Telli2016
SigMA
56%
44%
+
-
+
-
+
-
116
26
136
6
29
83
74
38
Agreement
78.3%
68.5%
Kappa
0.56
0.32

Figure 3

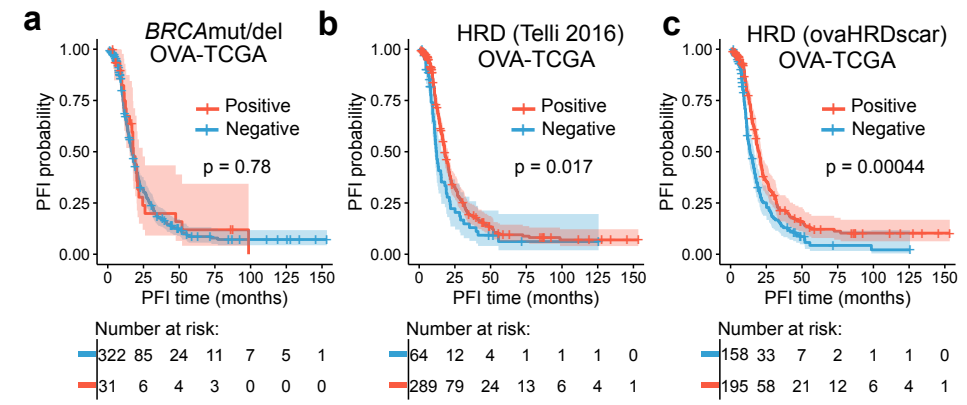

d *Cox model of PFS adjusted for residual tumor*

	OVA-TCGA n=353				OVA-TCGA* n=260				HERCULES n=33			
All samples:	N	Prop	HR	Pval	N	Prop	HR	Pval	N	Prop	HR	Pval
BRCAmut/del	31	9%	0.86	6.3e−04	0	0%	NA	NA	5	15%	0.66	0.082
Telli2016	289	82%	0.58	2.7e−06	208	80%	0.52	1.4e−05	23	70%	0.68	0.063
Tacaya2020	166	47%	0.63	1.2e−06	106	41%	0.60	4.5e−05	14	42%	0.49	0.029
ovaHRDscar	195	55%	0.59	1.5e−07	131	50%	0.54	2.8e−06	16	48%	0.37	0.013
*BRCA*mut/del excluded:	n=322				n=260				n=28			
Telli2016	258	80%	0.59	7.7e−06	208	80%	0.52	1.4e−05	18	64%	0.70	0.240
Tacaya2020	141	44%	0.63	5.7e−06	106	41%	0.60	4.5e−05	9	32%	0.54	0.160
ovaHRDscar	168	52%	0.59	6.1e−07	131	50%	0.54	2.8e−06	11	39%	0.39	0.078

Hazard-ratio (HR): 0.8 0.7 0.6 0.5 0.4

-log10(Pval): 4 5 6 | -log10(Pval): 4.4 4.8 5.2 | -log10(Pval): 0.9 1.2 1.5 1.8

**Excluding patients used for ovaHRDscar optimization*

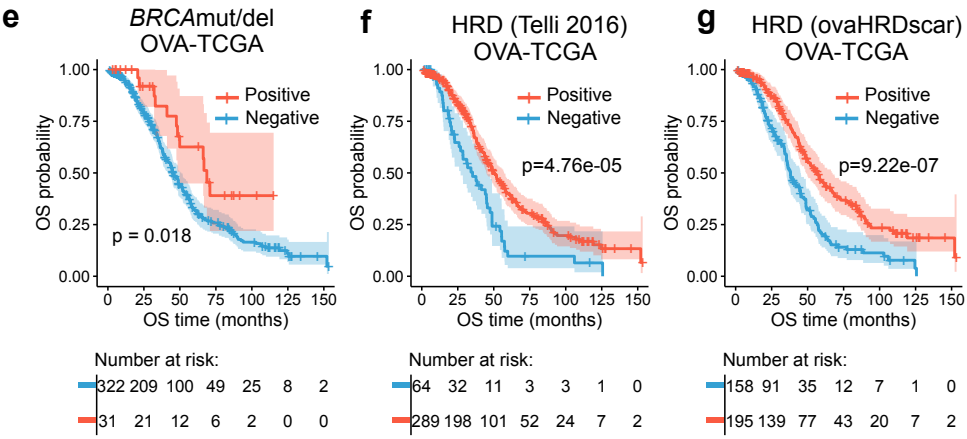

h *Cox model of OS adjusted for age at diagnosis*

	OVA-TCGA n=353				OVA-TCGA* n=260				PCAWG n=60			
All samples:	N	Prop	HR	Pval	N	Prop	HR	Pval	N	Prop	HR	Pval
BRCAmut/del	31	9%	0.55	3.7e−04	0	0%	NA	NA	13	22%	0.50	0.097
Telli2016	289	82%	0.52	1.1e−06	208	80%	0.48	5.5e−06	43	72%	0.51	0.067
Tacaya2020	166	47%	0.57	9.9e−07	106	41%	0.52	8.0e−06	20	33%	0.60	0.160
ovaHRDscar	195	55%	0.53	7.8e−08	131	50%	0.48	5.0e−07	28	47%	0.47	0.026
*BRCA*mut/del excluded:	n=322				n=260				n=47			
Telli2016	258	80%	0.54	5.5e−06	208	80%	0.48	5.5e−06	30	64%	0.59	0.220
Tacaya2020	141	44%	0.58	3.7e−06	106	41%	0.52	8.0e−06	11	23%	1.10	0.710
ovaHRDscar	168	52%	0.53	1.8e−07	131	50%	0.48	5.0e−07	17	36%	0.60	0.250

Hazard-ratio (HR): 0.8 0.7 0.6 0.5 0.4

-log10(Pval): 4 5 6 7 | -log10(Pval): 5.1 5.4 5.7 6.0 6.3 | -log10(Pval): 0.4 0.8 1.2

**Excluding patients used for ovaHRDscar optimization*

Figure 4

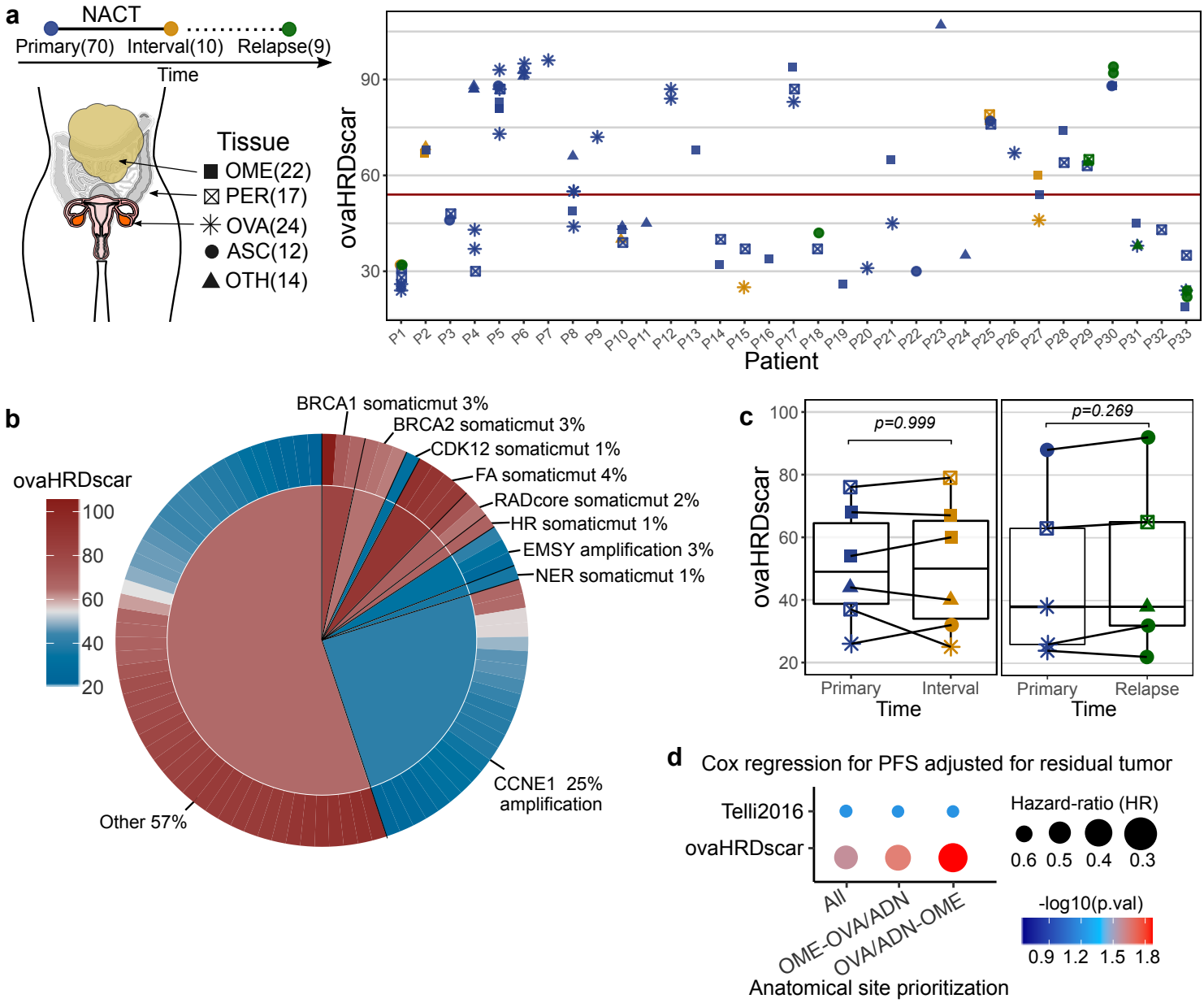
a
NACT
Primary(70)
Interval(10)
Relapse(9)
Time
Tissue
OME(22)
PER(17)
OVA(24)
ASC(12)
OTH(14)
ovaHRDscar
Patient
b
ovaHRDscar
BRCA1 somaticmut 3%
BRCA2 somaticmut 3%
CDK12 somaticmut 1%
FA somaticmut 4%
RADcore somaticmut 2%
HR somaticmut 1%
EMSY amplification 3%
NER somaticmut 1%
CCNE1 25% amplification
Other 57%
c
p=0.999
p=0.269
ovaHRDscar
Primary
Interval
Relapse
Time
d
Cox regression for PFS adjusted for residual tumor
Telli2016
ovaHRDscar
All
OME-OVA/ADN
OVA/ADN-OME
Anatomical site prioritization
Hazard-ratio (HR)
0.6 0.5 0.4 0.3
-log10(p.val)
0.9 1.2 1.5 1.8

Figure 5

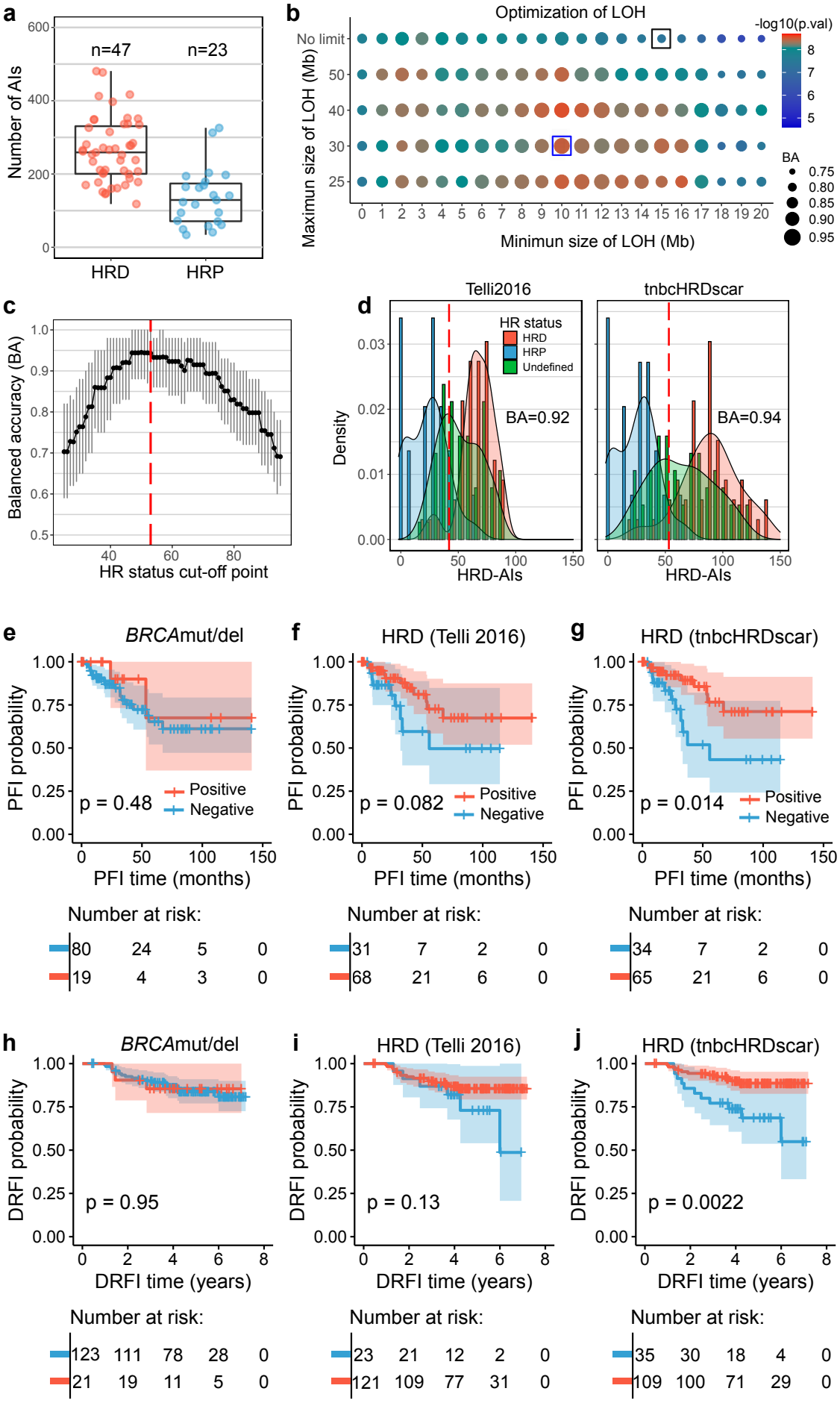
a
Number of AIs
n=47
n=23
HRD
HRP
b
Optimization of LOH
-log10(p.val)
Maximun size of LOH (Mb)
Minimun size of LOH (Mb)
BA
c
Balanced accuracy (BA)
HR status cut-off point
d
Telli2016
tnbcHRDscar
HR status
HRD
HRP
Undefined
BA=0.92
BA=0.94
Density
HRD-AIs
e
BRCAmut/del
PFI probability
p = 0.48
Positive
Negative
PFI time (months)
Number at risk:
80 24 5 0
19 4 3 0
f
HRD (Telli 2016)
p = 0.082
31 7 2 0
68 21 6 0
g
HRD (tnbcHRDscar)
p = 0.014
34 7 2 0
65 21 6 0
h
DRFI probability
p = 0.95
DRFI time (years)
123 111 78 28 0
21 19 11 5 0
i
p = 0.13
23 21 12 2 0
121 109 77 31 0
j
p = 0.0022
35 30 18 4 0
109 100 71 29 0

Supplementary Figure 1

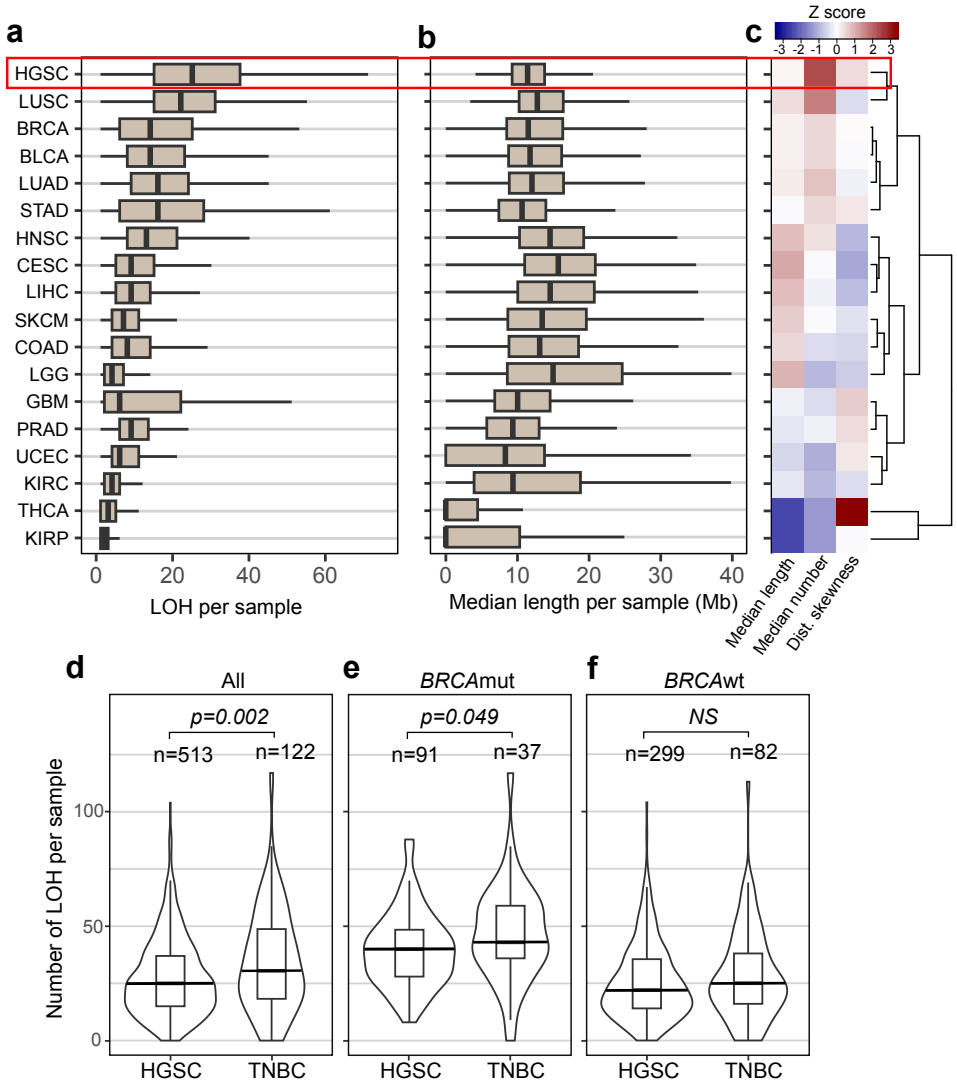

Supplementary Figure 2

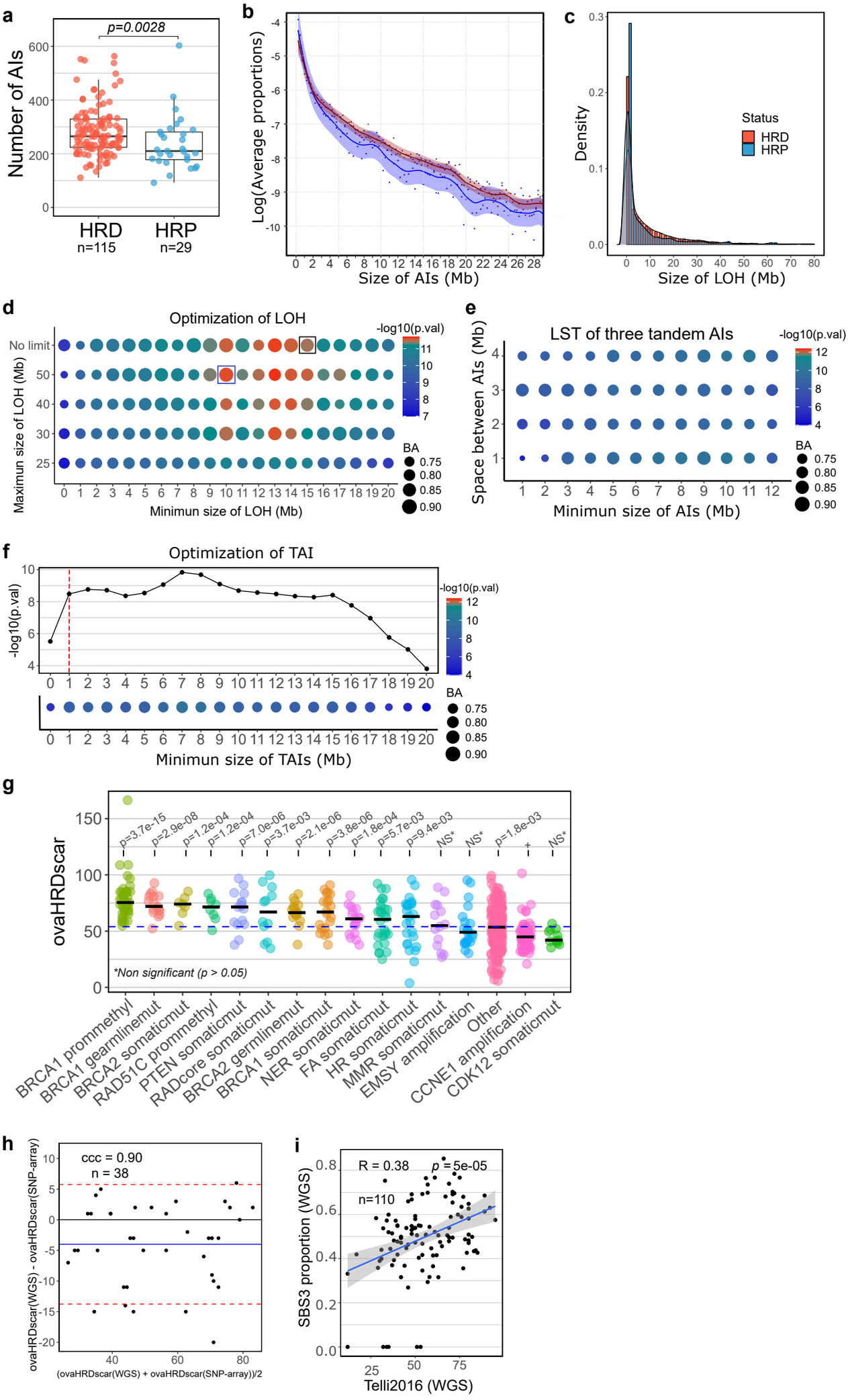

Supplementary Figure 3

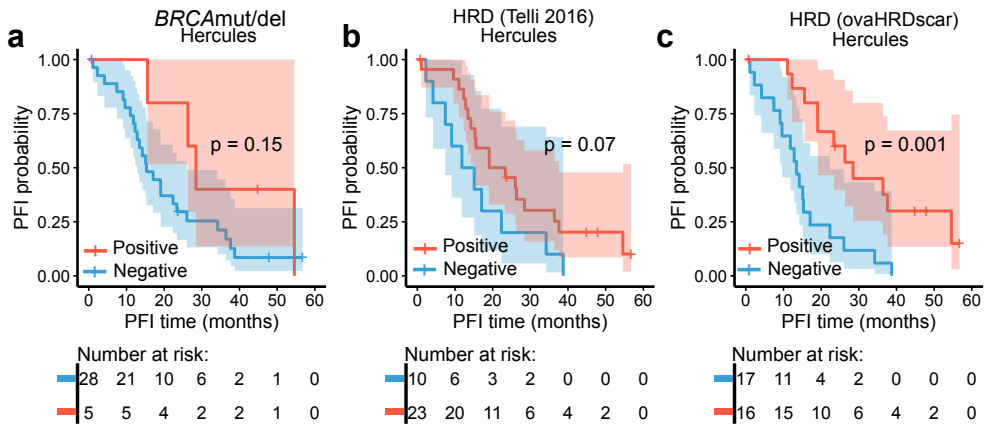

d *Cox model of PFS*

	OVA-TCGA n=353				OVA-TCGA* n=260				HERCULES n=33			
All samples:	N	Prop	HR	Pval	N	Prop	HR	Pval	N	Prop	HR	Pval
BRCAmut/del	31	9%	0.94	0.78000	0	0%	NA	NA	5	15%	0.46	0.1600
Telli2016	289	82%	0.69	0.01700	208	80%	0.64	0.01100	23	70%	0.49	0.0750
Tacaya2020	166	47%	0.67	0.00093	106	41%	0.63	0.00150	14	42%	0.36	0.0150
ovaHRDscar	195	55%	0.65	0.00049	131	50%	0.61	0.00046	16	48%	0.28	0.0019
*BRCA*mut/del excluded:	n=322				n=260				n=28			
Telli2016	258	80%	0.69	0.01900	208	80%	0.64	0.01100	18	64%	0.59	0.2000
Tacaya2020	141	44%	0.66	0.00110	106	41%	0.63	0.00150	9	32%	0.43	0.0850
ovaHRDscar	168	52%	0.64	0.00048	131	50%	0.61	0.00046	11	39%	0.33	0.0150

Hazard-ratio (HR): 0.8 0.7 0.6 0.5 0.4
-log10(pval): 1 2 3 | 2.0 2.5 3.0 | 1.0 1.5 2.0 2.5

**Excluding patients used for ovaHRDscar optimization*

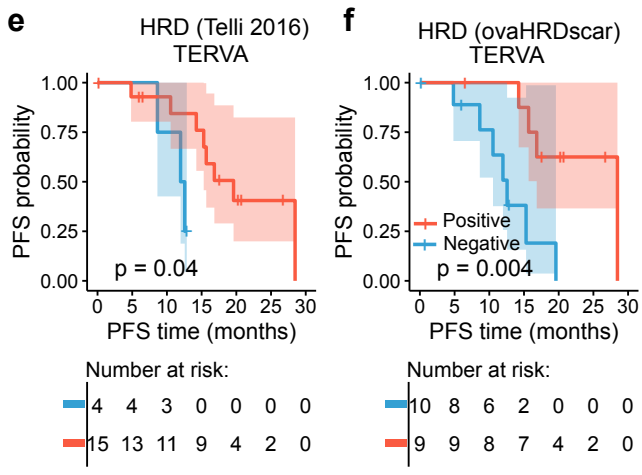

g *Cox model of PFS adjusted for residual tumor*

	TERVA n=19			
	N	Prop	HR	Pval
Telli2016	15	79%	0.189	0.18
Tacaya2020	7	37%	0.433	0.47
ovaHRDscar	10	47%	0.119	0.03

Hazard-ratio (HR): 0.1 0.2 0.3 0.4
-log10(pval): 0.6 0.9 1.2 1.5

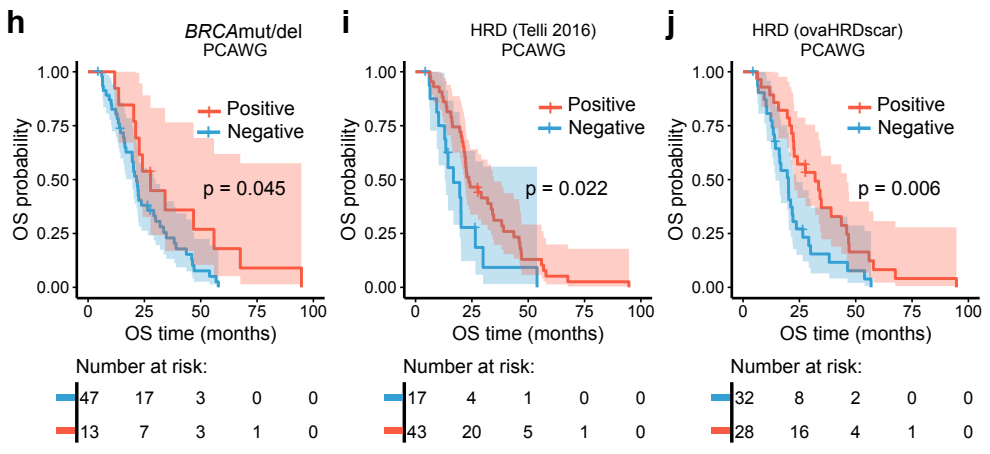

k *Cox model of OS*

	OVA-TCGA n=353				OVA-TCGA* n=260				PCAWG n=60			
	N	Prop	HR	Pval	N	Prop	HR	Pval	N	Prop	HR	Pval
BRCAmut/del	31	9%	0.50	2.0e−02	0	0%	NA	NA	13	22%	0.50	0.0490
Telli2016	289	82%	0.51	6.5e−05	208	80%	0.49	9.7e−05	43	72%	0.48	0.0240
Tacaya2020	166	47%	0.54	1.1e−05	106	41%	0.50	3.9e−05	20	33%	0.58	0.0710
ovaHRDscar	195	55%	0.52	1.4e−06	131	50%	0.48	4.3e−06	28	47%	0.46	0.0072
*BRCA*mut/del excluded:	n=322				n=260				n=47			
Telli2016	258	80%	0.54	3.0e−04	208	80%	0.49	9.7e−05	30	64%	0.57	0.0970
Tacaya2020	141	44%	0.55	4.4e−05	106	41%	0.50	3.9e−05	11	23%	0.98	0.9500
ovaHRDscar	168	52%	0.52	3.0e−06	131	50%	0.48	4.3e−06	17	36%	0.58	0.1000

Hazard-ratio (HR): 0.8 0.7 0.6 0.5 0.4
-log10(pval): 2 3 4 5 | 4.5 5.0 | 0.5 1.0 1.5 2.0

**Excluding patients used for ovaHRDscar optimization*

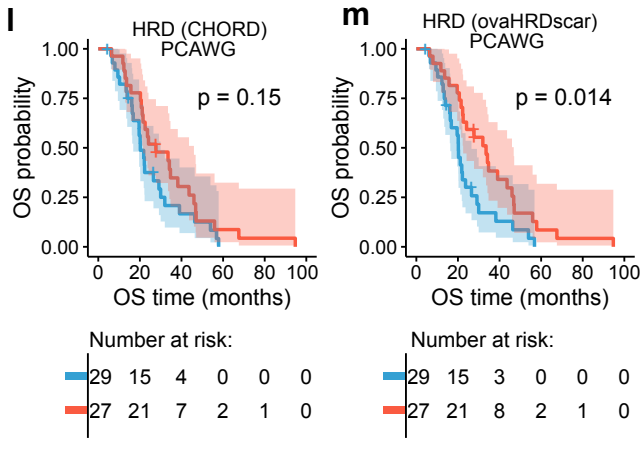

n *Cox model of OS*

	PCAWG n=56			
	N	Prop	HR	Pval
CHORD	27	48%	0.66	0.15
ovaHRDscar	27	48%	0.49	0.02

Hazard-ratio (HR): 0.7 0.6 0.5 0.4
-log10(pval): 1.0 1.2 1.4 1.6

Supplementary Figure 4

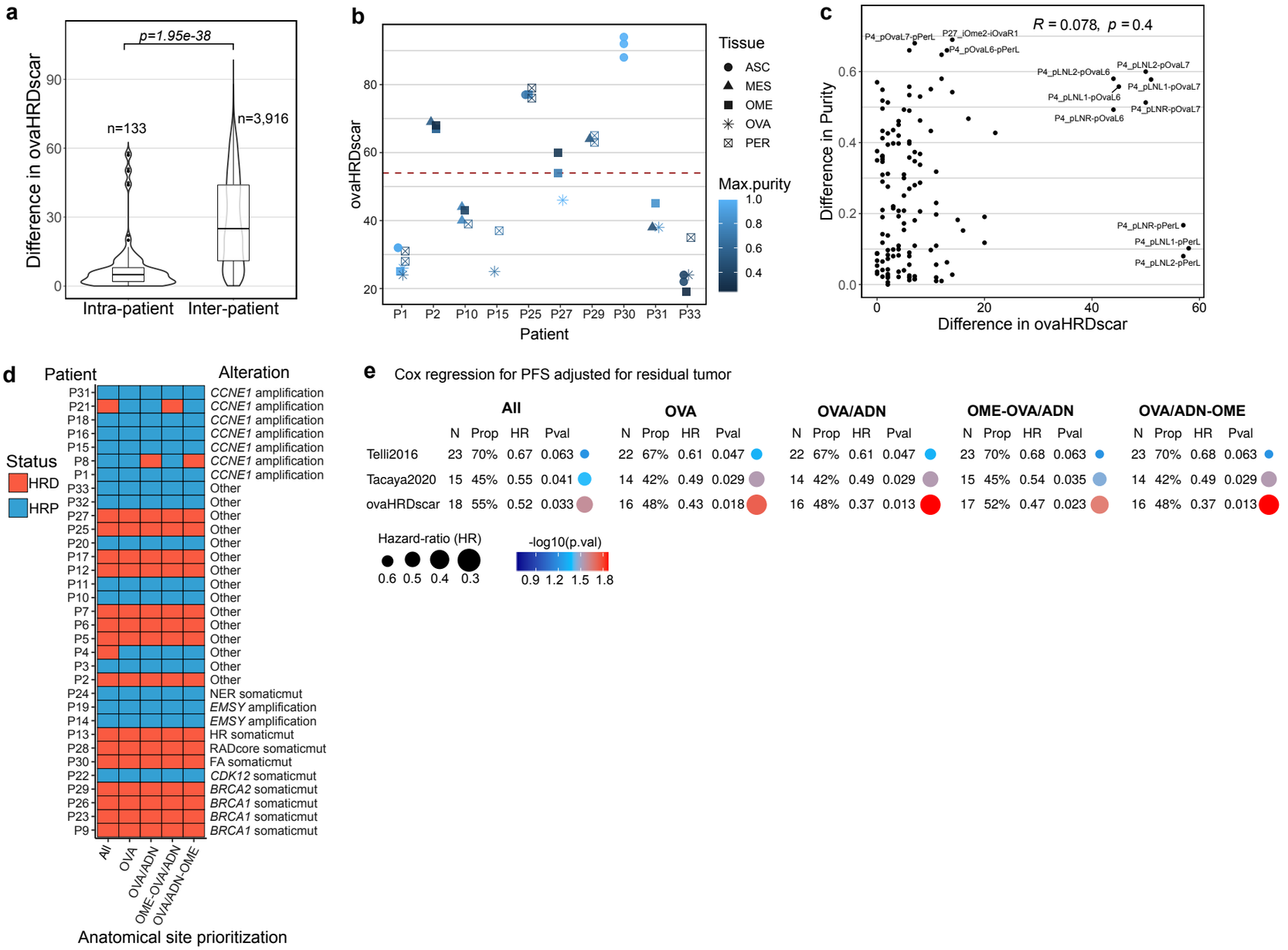
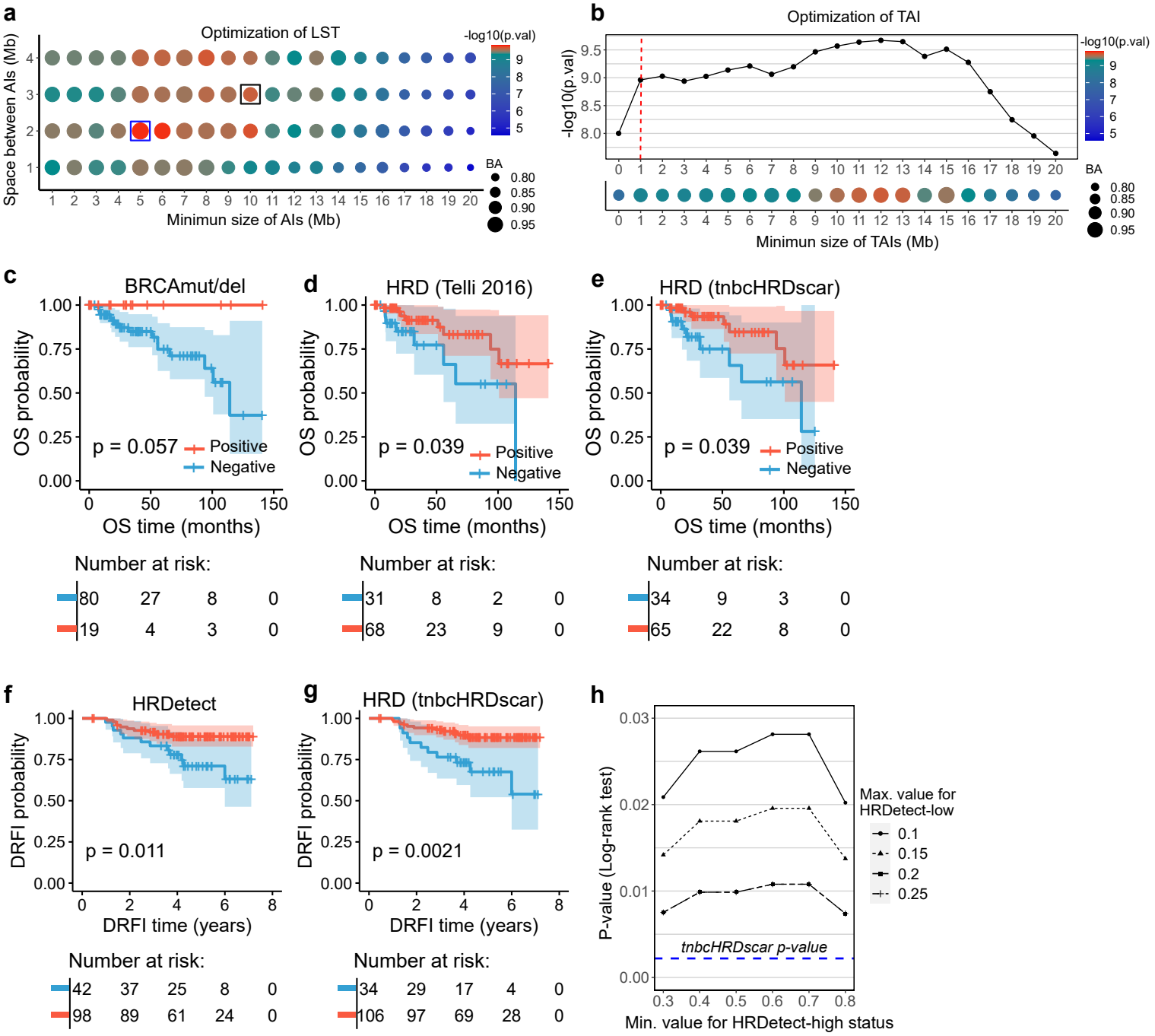
Supplementary Figure 5